Review article

Ragone plots revisited: A review of methodology and application across energy storage technologies

Inga Beyers, Astrid Bensmann *, Richard Hanke-Rauschenbach

Leibniz University Hannover, Institute of Electric Power Systems, Appelstraße 9A, Hannover, 30167, Germany

ARTICLE INFO

ABSTRACT

The term "Ragone plot" refers to a popular and helpful comparison framework that quantifies the energy–power relationship of an energy storage material, device, or system. While there is consensus on the general Ragone plot concept, many implementations are found in the literature. This article provides a systematic and comprehensive review of the Ragone plot methodology in the field of electric energy storage. A faceted taxonomy is developed, enabling existing and future Ragone plots to be unambiguously classified and contextualized. This review focuses on disseminating the methodology, discussing technology-specific aspects, and giving an overview of the further sizing and design methods developed based on Ragone plots. Additionally, this article identifies best practices for obtaining and presenting Ragone plots. This review is not limited to electrochemical energy storage, where the framework is traditionally applied, but also encompasses all other electric energy storage. Here, the Ragone plot can compactly quantify off-design performance and operational flexibility, independent of technology-specific performance indicators. This review is the first of its kind and can, therefore, guide future application of the Ragone plot framework in a consistent manner.

1. Introduction

This paper is a systematic review of the Ragone plot framework in the field of electric energy storage technologies. A Ragone plot is a characterization method for energy storage. Essentially, it shows the non-linear relationship between the energy that can be extracted from the storage and the discharge power. This energy–power relation contained in a Ragone plot can also be expressed through specific values (energy/power densities) or normalized values.

The Ragone plot is a useful framework and merits a more comprehensive, systematic application. It concisely demonstrates the energy–power relationship and its underlying characteristic trade-off between available energy E and discharge power P for a specific electric energy storage. It has a practical value in quantifying the off-design performance of a storage system in a constant-power regime (such as the electric grid). It can form the basis for further energy-storage-related methods, such as sizing and optimization methods. Additionally, it has a substantial teaching value, as a storage technology's underlying physical mechanisms determine the Ragone plot's characteristic shape.

This type of diagram was first introduced in 1968 in a seminal publication by David Ragone [1]. The diagram included empirically determined Ragone curves for various battery chemistries of the day; see Fig. 1. The type of diagram and its name soon established itself as a general concept and was applied in battery publications through the

1970s and 1980s, e.g., [2–5]. The 1990s saw an uptick in the usage of Ragone plots, concurrent with major progress in lithium-ion battery (LIB) and supercapacitor (SC) development. These were predominantly experimental Ragone plots to characterize self-assembled cells, e.g., [6, 7].

Pell and Conway were the first to provide a dedicated methodological ansatz to obtain Ragone plots for batteries and supercapacitors [8]. It consists of a pair of algebraic equations, including kinetic polarization via a Tafel relation and ohmic resistance as loss mechanisms. In 2000, Christen and Carlen [9] provided a theoretical framework for Ragone relations, based on a generally applicable differential equation that can be solved to a closed-form expression. It was applied to batteries, supercapacitors, and superconducting magnetic energy storage (SMES). This influential publication laid a solid foundation for further theoretical and experimental work on Ragone relations. At the same time, the first Ragone plot characterizations of commercial lithium-ion [10,11] and supercapacitor cells [12,13] were carried out.

With the concept established, two dimensions can be differentiated in further research from 2000 onward: (I) pure application of the Ragone plot concept for energy storage characterization and (II) the Ragone plot and its methodology and application as a subject of research itself, with the latter being of higher interest for this review.

Nomenclature

Symbols

$\ddot{s}$	Mass point acceleration
$\dot{q}$	Heat transfer rate
$\dot{s}$	Mass point speed
η	Electric efficiency
ψ	Mechanical Potential
τ	Friction time constant
C	Capacitance
E	Available energy
e	Energy density
F	Force
I	Current
L	Inductance
m	Mass
P	Charge/discharge power
p	Power density
Q	Charge
R	Resistance
s	Mass point coordinate
T	Temperature
t	Time
U	Voltage
V	Electrochemical Potential
v	Volume

Indices

0	Open-circuit
ave	Average
fin	At final time
ini	At initial time
max	Maximum
min	Minimum
m	Gravimetric
th	Thermal
UI	Switch point voltage to current termination
vol	Volumetric
cell	Characteristic of an electrochemical cell
demand	Demand from storage application

Acronyms

ASS	All solid state
CAES	Compressed air energy storage
CC	Constant current
CGES	Compressed gas energy storage
CP	Constant power
CR	Constant resistance
DFN	Doyle–Fuller–Newman
ECM	Equivalent circuit model
FES	Flywheel energy storage
HES	Hydrogen energy storage
HESS	Hybrid energy storage
HPPC	Hybrid pulse power characterization
LAB	Lead–acid batteries
LCO	Lithium-cobalt-oxide
LFP	Lithium iron phosphate

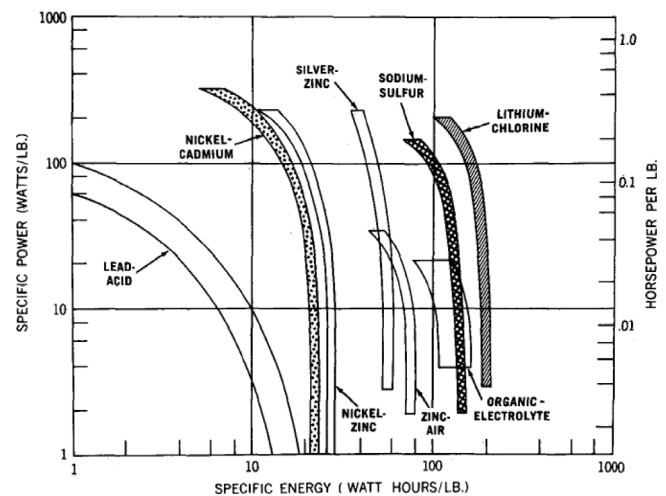|	
LIB	Lithium-ion battery
LSB	Lithium-sulfur batteries
LTO	Lithium-titanium-oxide
NCA	Nickel cobalt aluminium oxide
NMC	Nickel-manganese-cobalt
NMH	Nickel-metal-hydride
PCM	Phase change material
PTES	Pumped thermal energy storage
RC	Resistance-capacitance
SC	Supercapacitor
SMES	Superconducting magnetic energy storage
TES	Thermal energy storage

Fig. 1. The original diagram of the gravimetric energy density – gravimetric power density relations of various battery chemistries, presented by D. Ragone in 1968. Used with permission of SAE International, from [1]; permission conveyed through Copyright Clearance Center, Inc.

Regarding dimension (I), the Ragone plot has established itself as a standard framework among performance reporting tools for new electrode materials and cell chemistries of batteries and supercapacitors [14]. Here, several overarching trends are reflected in Ragone plot usage. As conventional lithium-ion batteries reach their practical and theoretical performance limit, two main avenues of improvement are being explored, namely substituting conventional graphite anode material with various metal anodes [15] and using solid-state electrolytes instead of conventional liquid electrolytes [16]. Additionally, lithium-free chemistries based on metals such as Mg, Ca, and Al are being explored [17]. In the field of supercapacitors, the focus lies on improving conventional carbon-based electrodes [18,19], developing new electrode materials, e.g., metal-oxides or polymers [20], and improving the voltage window and stability of electrolytes [21]. Supercapacitor-battery hybrids are also increasingly studied, closing the gap between the respective technologies [22,23].

Other energy storage technologies are historically not characterized via Ragone plots. However, in recent years they have been applied for the first time for compressed air energy storage (CAES) [24], compressed gas energy storage (CGES) [25], hydrogen energy storage (HES) [26], flywheel energy storage (FES) [27,28], thermal energy storage (TES) [29,30] and pumped thermal energy storage (PTES) [31]. Ragone plots have also been applied outside of electric energy storage to characterize power sources such as combustion engines, photovoltaic cells and fuel cells [32], radioisotope cells [33] and desalination processes [34].

In terms of dimension (II), it is notable that the Ragone plot has been incorporated into numerous proposed storage design methods, particularly for hybrid energy storage systems [35–39], as well as specialized electrified vehicles, such as trolleybuses [40], warships [41] and military vehicles [42]. The Ragone plot describes a fundamental relation at the terminals of the storage component/system and is thus well-suited for initial technology selection and sizing problems.

While the common understanding is that a Ragone plot shows an energy–power relation, this is where the consensus stops. Even though there is a large body of literature on Ragone plots, there is ambiguity and variety regarding the methodology, utilization and visual presentation. The term is loosely applied, and Ragone curves from different publications can rarely be compared directly. This ambiguity and variety can be captured and highlighted in a systematic review, where the research community will benefit from clear and distinct classification terminology and possible convergence of practices. This work is the first such systematic review of Ragone plots.

Our review paper will, therefore, deliver the following contributions:

1. Bringing order and system to the Ragone plot concept by developing a general taxonomy for classifying all aspects of Ragone plots of electric energy storage.
2. Comprehensive and holistic analysis of Ragone plots by systematically reviewing the literature, utilizing the developed taxonomy.
3. Identification of best practices so that energy storage performance can be reported via Ragone plots consistently and not suffer misrepresentation.

The paper is structured as follows: Section 2 describes materials and method, where Section 2.1 outlines the literature method applied and Section 2.2 introduces a taxonomy to classify Ragone plots. The subsequent analysis in Section 3 is structured via this taxonomy. Section 4 concludes the review.

2. Materials and methods

2.1. Literature method

"Ragone plot" is a common term with a high level of adoption, as evidenced by ca. 26.300 Google Scholar search results (as of 11.04.23). To narrow this down, the focus of this review lies on finding literature that covers the Ragone plot method as the subject of research itself, representative papers of a specific Ragone plot type, interesting/novel applications to new energy storage subfields, methods based on Ragone plots and other seminal papers in the field.

The basis of the literature search was conducted through a targeted search query in the Scopus database. Here, the terms "Ragone plot" and "Ragone diagram" were searched in the title, abstract, or keywords of publications, as this signals a higher level of engagement with the concept. The search resulted in 297 documents (as of 11.04.2023). Some publications were discarded based on scope, language and availability. Further documents were added through citation analysis and targeted Google Scholar searches. The final document selection includes 104 titles (83 journal papers, 14 conference papers, 7 other), which covers the variety of Ragone plots and their usage in literature. An overview of the literature sources is provided in the supplementary material; see Appendix.

2.2. Review framework

During the literature review, it was found that the implementation of Ragone plots is highly varied, and there is no single definition of what exactly constitutes a Ragone plot. In this review, we accept this variety and aim to distinguish, classify and bring order to this variety.

For this purpose, a Ragone plot taxonomy was developed during the review process. A taxonomy is a system by which knowledge can be organized and classified [43]. Two types of taxonomy are distinguished: the hierarchical and the faceted taxonomy. In the hierarchical taxonomy, classification categories are nested into one another and organized into a hierarchical structure. In a faceted taxonomy, knowledge is classified via multiple aspects, referred to as "facets". These facets apply to the subject independently, and there is no hierarchical relationship between them [43].

A faceted taxonomy was found to be most suitable to classify Ragone plots of electric energy storage. A first version of the taxonomy was developed during the initial scoping of the literature. This first version was further refined and iteratively reworked in the review process, resulting in the final version in Table 1. Seven facets were identified that characterize Ragone plots, which provide the structure for the analysis in Section 3, namely representation level, hierarchical level, method, technology, process direction, visualization and utilization. Every facet contains a different number of "classifiers", which are the different options that apply to this facet. The taxonomy is given in Table 1 and discussed in detail in the following section.

3. Analysis via Ragone plot taxonomy

The following section will analyze the different facets of Ragone plots in the order presented in Table 1.

3.1. Representation level

Ragone plots found in the literature contain four elements: characteristic curves, enveloping bands, nominal points and arbitrary shapes. An example from literature is shown for each element in Fig. 2, but it must be noted that they can also be combined freely within a single Ragone plot. These elements all differ in what they represent and thus the level of information they contain: single storage or whole technologies, single operating points or entire operating ranges. We therefore distinguish four different "representation levels", discussed in detail in the following.

The first representation level is the classic Ragone curve, which is most commonly found in literature and shown as an example in Fig. 2(a) from [36]. It is a single characteristic curve that shows the energy–power trade-off for a specific storage instance of a particular technology. In the example, the Ragone curves are obtained for a commercial supercapacitor cell (Maxwell) and lead acid battery (Moura). The Ragone curve is a limit curve that marks the outer limit of the feasible operating area for the specific storage. Ragone curves are sometimes called "E-P curves", particularly when absolute energy and power values are plotted [46]. In the chosen example, specific values are used, but this is not always the case.

Combining several Ragone curves into enveloping characteristic bands represents the range of energy and power values an entire storage technology can take up, which is the second possible representation level. An example from [44] is shown in Fig. 2(b), with enveloping bands for four different electrochemical storage technologies. The width of the technology band can be chosen from empirical experience [1] or other sources, e.g., product data sheets [44]. Enveloping bands are the type of representation used in the original publication by D. Ragone in 1968 [1]. The example in Fig. 2(b) also includes isochrones, which are diagonal lines representing all points with the same discharge duration in the E-P plane. Isochrones help to quickly assess discharge durations and the relative position of a storage technology with respect to other technologies.

In some cases, Ragone plots contain only a single operating point of a single storage instance, often the nominal point. This is the third possible representation level. An example taken from [39] in Fig. 2(c) contains a selection of commercially available lithium-ion cells from

Table 1
Faceted taxonomy to classify Ragone plots of electric energy storage.

| Facet	Classifiers			
Representation level	Single storage instance represented by a characteristic curve	Entire storage technology represented by an enveloping band	Single storage instance represented by a single operating point	Entire storage technology represented by an arbitrary shape
Hierarchical level	Material level		Component level	System level
Method	Experimental		Model-based	Datasheet-based
Technology	Li-ion batteries (LIB) Lead-acid batteries (LAB) Redox flow batteries (RFB) Nickel metal-hydride batteries(NMH) Lithium-sulphur batteries (LSB) Supercapacitors (SC) Superconducting magnetic energy storage (SMES) Compressed air energy storage (CAES) Hydrogen energy storage (HES) Flywheel energy storage (FES) Pumped thermal energy storage (PTES) Hybrid energy storage sytems (HESS)			
Process direction	Charge		Discharge	
Visualization	Energy over power		Power over energy	
	Specific values (gravimetric)	Specific values (volumetric)		Absolute values
	Normalised to a reference value of E & P		Not normalised	
	Logarithmic	Linear	Semilog (energy)	Semilog (power)
Utilization	Visualization & comparison	Optimization constraint		Graphical sizing method

a) Single storage instance represented by a characteristic curve
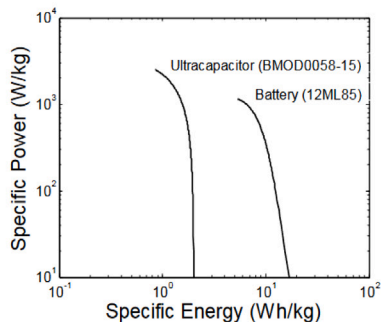
b) Entire storage technology represented by an enveloping band
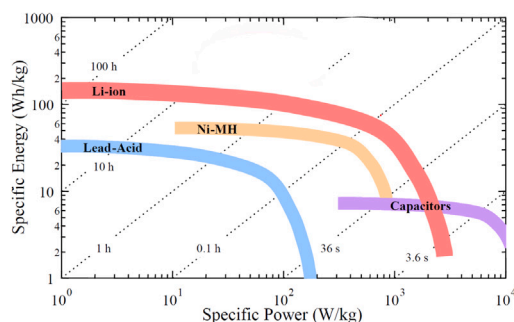
c) Single storage instance represented by a single operating point
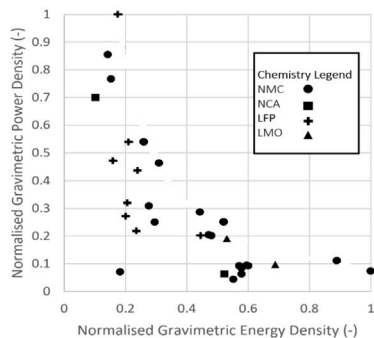
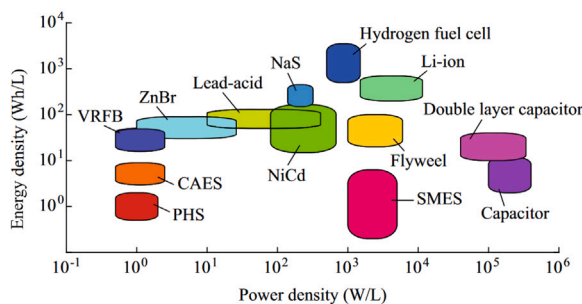**d)** Entire storage technology represented by an arbitrary shape

Fig. 2. Example figures for the different possible representation levels. Subfigure (a) ©2011 IEEE. Reprinted, with permission, from [36]. Subfigure (b) used with permission of the American Institute of Physics, from [44]; permission conveyed through Copyright Clearance Center, Inc. Subfigure (c) modified from [39], licensed under CC BY 4.0. Subfigure (d) modified from [45], licensed under CC BY 4.0.

four different chemistries, where each cell is represented by a single, nominal E-P value pair.

To represent an entire technology, an arbitrary shape in the E-P plane can be used, as shown in Fig. 2(d), from [45]. This fourth representation level shows the typical order of magnitude of E, P or derived specific quantities of a technology. The shapes and their location are commonly chosen from experience or manufacturer's information. In some cases, multiple nominal points are explicitly encompassed into one summarizing shape, a "nominal area" of sorts [47]. The shapes are typically squares or circles/ovals, but trapezoids or other forms are sometimes used. All arbitrary shapes must be understood as rough guidelines.

The latter two representation levels do not contain the information of a classic characteristic Ragone curve and thus do not have all the advantages listed at the outset of the introduction. There is also no extensive methodology required beyond processing the manufacturer's information. However, they still contain information about an energy–power relationship, and ultimately, the name "Ragone plot" has long been applied to these types of representation levels by the respective authors themselves. There is, therefore, no reason to exclude them from this review or the developed taxonomy.

3.2. Hierarchical level

Energy storage can be analyzed on different scales, referred to as "hierarchical levels" in the presented taxonomy (Table 1). Here, three levels are possible: material level, component level and system level, a distinction also found in other literature [48,49].

The different hierarchical levels can be illustrated by considering cell-based electrochemical storage technologies, i.e., batteries and supercapacitors. At the material level, the energy–power relation of a specific electrode is studied, e.g., a particular active material or the effect of non-active material (binder, additives) or adjustments to the electrode architecture (structuring, porosity). The electrodes are typically implemented as a half-cell and then combined with a reference electrode to form a full cell, often in a lab-built, prototypic setup [50]. At the component level, the complete and sealed cell with housing, current collector tabs, separator, electrolyte, gaskets and poles is studied. These are most often commercially available cells. At the system level, the E-P relation of a system is studied, consisting of multiple cells connected in series and parallel into one or more modules and including necessary periphery, such as a heating/cooling system, electronic monitoring and control, and power electronics.

This distinction between material/component/system is equally applicable in, e.g., thermo-mechanical energy storage. A material-level Ragone plot shows the E-P relation inherent to a specific material, for example, heat stored in a specific phase-change material. The component level considers a fully functional component, such as a thermal energy storage with an integrated heat exchanger. In contrast, a system-level Ragone plot analysis would consider the complete storage system with multiple components and energy conversion steps.

In hybrid energy storage systems (HESS), combining two storages can occur on any hierarchical level. For example, [51–54] characterize battery-supercapacitor HESS that combine individual battery and supercapacitor cells in configurations that best match up the voltage levels of the respective technologies. These are component-level HESS. However, recent research is more focused on material-level HESS, where a battery electrode and a supercapacitor electrode are combined to form a single hybrid cell [22]. This trend is increasingly blurring the lines between batteries and supercapacitors in the quest to combine the advantages of both technologies.

Both the Ragone plot outcome and the framework's prevalence differ between these hierarchical levels, as illustrated by way of lithium-ion batteries with nickel–manganese–cobalt (NMC) chemistries in Fig. 3. The achievable gravimetric energy density reduces from material to component (cell) to system level as more inactive material is incorporated in each level. While the qualitative shape at the material and cell level is similar, this cannot be formulated as a general rule, and other technologies could differ in this respect.

System-level Ragone curves are generally lacking, and only the nominal operating points of three automotive systems are included for reference in Fig. 3. Very few publications address system-level Ragone plots of any technology, and when they do, it is often experimental work on prototypic systems, e.g., [24,25]. Due to high costs, system-level experiments of large engineering systems are rarely performed [60]. Model-based analysis offers an alternative here, however, for some emerging storage technologies such as liquid air energy storage (LAES) or PTES, comprehensive, system-level models are still rare or lacking [61,62].

Material research for electrochemical energy storage has embraced the Ragone plot as a standard framework among the field's typical reporting tools/methods [14,63]. This is especially true for supercapacitors — most publications containing Ragone plots at the material level deal with supercapacitor electrode material. Here, many increasingly specific electrode material variations have been studied and characterized with the help of Ragone plots, with the motivation to increase energy density. However, a deeper analysis is not expedient for this review.

The translation of material-level performance to cell-level performance remains a perpetual issue in electrochemical energy storage, addressed for Zinc-based batteries by [64], all-solid-state lithium batteries by [16], lithium-ion batteries by [50] and for supercapacitors by [63,65–67]. Spectacular Ragone plot results for new active material or electrode architectures at the material level rarely translate to superior cell-level performance [50]. The problem lies in erroneous or intentionally misleading extrapolation to cell level, which is extenuated by a lack of standardization for performance reporting [65,66]. However, this cannot be construed as a critique of Ragone plots per se and can be easily remedied by clearly separating hierarchical levels [63] and not inferring material-level performance to component (cell) level via overly optimistic methods.

One notable example to combat this problem is found in [50]. Here, a tool called the "Ragone calculator" is provided to extrapolate material-level to cell-level performance for lithium-ion batteries in a structured and transparent manner. After entering the rate capability result obtained from the half-cell and the geometry of the studied electrodes, a standardized parameter set is applied to extrapolate to full-cell performance. Similar rules for translating material-level performance/rate capabilities to component-level and system-level performance should be established for other technologies by respective domain experts.

3.3. Method

Ragone plots can principally be derived in three different manners:

1. Experimental, i.e., by conducting a set of experiments
2. Model-based, i.e., by formulating and evaluating models
3. Datasheet-based, i.e., by processing only datasheet information

While model-based approaches often include experimental parametrization, this distinction is still considered practicable to classify the fundamental approaches to obtain a Ragone plot. Datasheet-based methods are both simpler and less extensive than the other two options. They are nevertheless included as a separate category because these provide quick alternative options, especially where resources are constrained. In this subsection, the three categories will be discussed one after the other, as presented in the taxonomy: first experimental, then model-based, then datasheet-based.
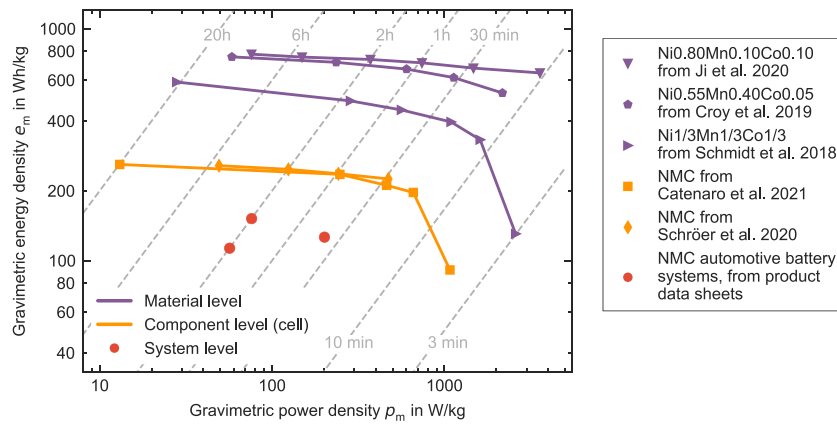
Fig. 3. Ragone plots of NMC-based lithium-ion batteries on different hierarchical scales, compiled from literature [55–59].

3.3.1. Experimental

The classic Ragone curve is obtained by performing multiple full charges/ discharges at different constant power levels and plotting the results in the energy–power plane. For the discharge direction, this is conducted as follows: Proceeding from a fully charged cell, device or system, the storage is discharged at a defined constant power P. The discharge lasts a finite time $t_{\mathrm{fin}}(P)$ until a predefined storage limit is reached, and the storage is unable to deliver the required constant power anymore [9]. This limit can relate to the potential variable of the storage, e.g., the minimum voltage U_{min} of a battery or minimum water level in pumped hydro energy storage. Alternatively, a flow variable limit (e.g., maximum current I_{max} of a supercapacitor or maximum mass flow in a compressed air system) or a safety limit such as a maximum temperature T_{max} can be reached. The available energy E then is the constant discharge power multiplied by the discharge time; see Eq. (1).

$$E(P) = P \cdot t_{\mathrm{fin}}(P) \qquad (1)$$

The constant power value P and its corresponding available energy $E(P)$ constitute a distinct point on the Ragone curve. The process is repeated for other power values while keeping the same operating limits. Consistency in operating limits is essential; indeed, the Ragone relation of an electrochemical cell would expressed more accurately as $E = f(P, U_{\mathrm{min}}, U_{\mathrm{max}}, I_{\mathrm{max}}, T_{\mathrm{max}})$ and the governing operating limits should always be reported.

If needed, the energy and power density based on either mass m or volume v of the storage can be calculated, giving the gravimetric energy density e_{m} and gravimetric power density p_{m} as

$$e_{\mathrm{m}} = \frac{E}{m} \qquad (2)$$

$$p_{\mathrm{m}} = \frac{P}{m} \qquad (3)$$

or the volumetric energy density e_{vol} and volumetric power density p_{vol} as

$$e_{\mathrm{vol}} = \frac{E}{v} \qquad (4)$$

$$p_{\mathrm{vol}} = \frac{P}{v}. \qquad (5)$$

The charge direction is characterized analogously to the discharge direction: the fully discharged energy storage is charged with a constant power for a finite time until the storage cannot accept the constant power anymore due to reaching an operating limit. The process is repeated for multiple different charge powers. Note: From this point, this subsection refers only to "discharge", even when the discussed point applies to the charging process as well, for the sake of brevity. The characteristic difference between charge vs. discharge is detailed in Section 3.5.

The experimental method of Ragone plots itself, and its influence on the outcome of the Ragone curve is typically not a point of discussion. The focus generally lies on the specific obtained results, and therefore, literature on experimental practices for obtaining Ragone plots is limited. Nevertheless, three relevant experimental aspects have been identified and will be discussed in the following subsections:

1. How to ensure that the Ragone plot range is captured sufficiently.
2. How the "hack" encountered in battery research, where constant-current results are converted into energy–power value pairs, compares to the classic approach described above, and what error this produces.
3. How pulsed discharges and HPPC tests have been used for Ragone plots.

Capturing the full Ragone curve. At high discharge powers, the available energy delivered by the energy storage drops due to polarization effects, inner friction or transport losses [28]. This drop can be more or less pronounced, depending on the technology and the operational limits imposed by the manufacturer or the user. It can also be accentuated through logarithmic visualization, further discussed in Section 3.6. Regardless, the aim should be to obtain the energy–power relation over a representative range, including the energy drop at high discharge powers, to have a meaningful basis for selecting an operating point. A suitable operating point is often located in the vicinity of the energy drop (referred to as the "knee" of the Ragone curve by [68]) because both energy and power have relatively high values [68].

Fig. 4 shows the characteristic shape of a complete Ragone curve for commercial lithium-ion cells from [46]. It shows a steadily decreasing available energy, as the constant discharge power increases until a specific point $P_{\mathrm{UI}} = U_{\mathrm{min}} \cdot I_{\mathrm{max}}$ is reached [46]. This point marks the power value at which the discharges switch from getting terminated due to reaching U_{min} to getting terminated due to reaching the maximum operating current I_{max}. In a constant-power (CP) discharge, the current drawn must increase as the cell voltage U drops and is at its highest at the end of the discharge. At low power values, this final current is below I_{max} and discharges are terminated by U_{min}. At high powers, the current can reach the cell's maximum current I_{max}, which prematurely terminates the discharge process and results in a drop in obtained energy.

To capture a relevant range of the Ragone plot, at least P_{UI} should be applied for a meaningful insight into the operational behavior for high discharge powers, as this marks the beginning of a significant energy drop. Testing equipment must be selected for this required discharge power. Equipment limitations as the sole reason behind the partial capture of a Ragone curve should be avoided. For example, in [69], the maximum power of the testing equipment used is 30 W, while
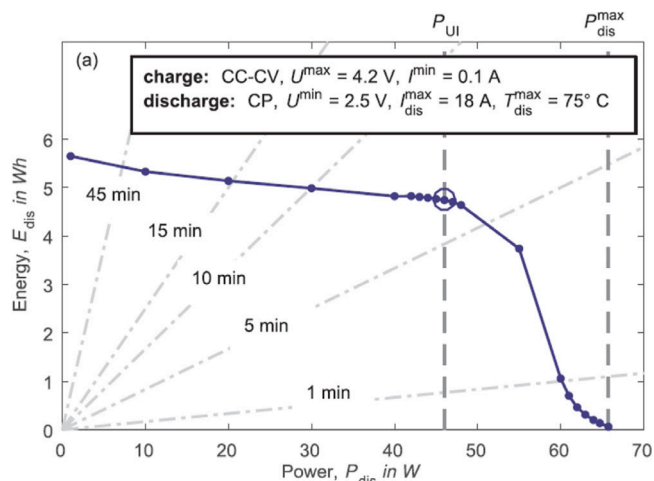
Fig. 4. Ragone plot of a commercial 18650-format lithium-ion cell with Nickel–Cobalt–Aluminum (NCA) chemistry at 25 °C via multiple constant-power discharges. Used with permission of Elsevier Science & Technology Journals, from [46] with minor edits; permission conveyed through Copyright Clearance Center, Inc.

the cells could be discharged with $P_{\mathrm{UI}} = 50\,\mathrm{W}$ and higher, all while keeping within manufacturer-specified limits. This results in a Ragone curve that covers approximately the first third of the complete Ragone curve shown in Fig. 4. In [70], a similar equipment-limit problem was circumvented by extrapolating experimental data points with the energy–power relation formulated by [9] for supercapacitors.

There is no consensus concerning the number of discharges needed to form a Ragone curve. In Fig. 4, the Ragone curve is composed of 20 discharges, which results in a high experimental effort. This large number is not necessary because the discharges are oversampled around P_{UI} and at $P > 60\,\mathrm{W}$ for didactic purposes. Balducci et al. [14] recommend reporting at least four different discharge points to accurately represent the energy–power relation and performance in the context of supercapacitors. This rule of thumb can be extended to all technologies.

Using adapted constant-current results. Characterization with a constant-current (CC) discharge is a common experimental practice in the field of electrochemical energy storage. CC discharge is a natural choice, because (I) manufacturers typically provide CC discharge data, thus CC tests are relevant for comparison to datasheets of commercially available cells, (II) standard tests, e.g characterizations performed according to vehicle IEC standards 62660 and aircraft standards DO-311, are typically CC tests [69] and (III) material-level cycle testing of electrochemical storage to obtain Ragone plots is almost exclusively performed with galvanostats, which apply a galvanostatic (CC) discharge [14].

There is thus a motivation to obtain Ragone plots from tests performed anyhow and thus not to have to perform additional CP discharges. This has led to the adaption of experimental CC discharge results for Ragone diagrams. The power varies throughout a CC discharge and, therefore, does not yield a single distinct power value that can be plotted in the E-P plane unambiguously. To circumvent this, the power is averaged for the discharge process with

$$P_{\mathrm{ave}}(I) = \frac{E(I)}{t_{\mathrm{fin}}} \tag{6}$$

and the available energy E [71] as

$$E(I) = \int_{t=0}^{t=t_{\mathrm{fin}}} U(t) \cdot I \, \mathrm{d}t. \tag{7}$$

While the equations above are valid for electrochemical energy storage technologies characterized by a voltage and a current, the analogy of different discharge modes can be transferred to other storage technologies. A discharge with constant current (CC) implies a constant flow variable. This discharge regime has equivalents in other technologies, e.g., a constant mass flow in compressed air energy storage or pumped hydro energy storage. This constant-flow discharge would differ in its energy–power relations from a constant-power discharge.

The different discharge modes (CP vs. CC) result in different Ragone curves for the same energy storage. This effect has not been widely addressed, except in three recent publications: in [72] for supercapacitors and [46,69] for lithium-ion batteries. Allagui et al. extensively studied the effect of three different loading conditions (CP/CC/CR) on the Ragone plot for commercial supercapacitor cells [72]. However, the Ragone plots in the publication are not presented classically, but rather as the instantaneous power and energy of a single discharge. Sarpal et al. demonstrated the effect of different reference voltages (mean, nominal, maximum, minimum) when converting CC results into Ragone plots [46]. Zhang et al. [69] experimentally demonstrate the difference between Ragone plot results obtained via CP and CC discharge. Their results indicate that CC discharge results in higher energy densities (up to 25%) than the CP discharge. In the publication, no explanation is put forward. However, the interested reader can refer to Fig. 5, where the model of Verbrugge and Ying [73] is evaluated for both CC and CP discharge. The figure explains the difference in available energy and energy density with an illustrative example.

An obvious implication of this difference in CP and CC discharge results is that the discharge mode needs to be clearly specified when reporting Ragone plots. Additionally, the research community should ideally perform CP discharge tests, even if these need to be conducted on top of standard CC tests because a CP discharge corresponds to the true power delivery capabilities of the energy storage. The calculated average power obscures the large power variations during a CC discharge. Ultimately, applications have a power requirement, not a current requirement, that the energy storage needs to deliver. While this power requirement might not be constant but rather a time-varying power profile, Christen argues in [31] that the full CP discharge of the Ragone plot "can serve as a simple, well-defined scenario to characterize different energy storage devices on equal footing".

Ragone plots via pulsed discharge and HPPC tests. Instead of a steady discharge, pulsed discharge has also been employed historically as a type of load from which Ragone plots can be obtained, see [51], [52] and [54]. Pulsed discharge introduces an additional mode of play into the already vast field of Ragone plot methodology. The motivation behind pulsed discharge is that a Ragone plot generated from a steady discharge cannot give information on highly dynamic cyclical loads. Pulsed power testing has been implemented as a remedy to systematically encode the effects of cyclical loading on energy–power relations of storage technologies.

A prominent example of an application that requires pulsed loads is hybrid-electric vehicles' start-stop cycles [54]. At this point, fully electric vehicles have been commercialized successfully, and pulsed power Ragone plots for hybrid electric vehicle applications have decreased in relevance. There has been no publication on the subject since 2010. Nowadays, highly dynamic, specific load profiles are typically evaluated individually and not integrated into a Ragone curve.

A special case of pulse power characterizations is hybrid pulse power characterization (HPPC), where a specific pulse protocol is observed, combining both charge and discharge, as specified in [74]. They have been applied, amongst others, in so-called "non-conventional" Ragone plots to characterize LIB cathode material in [75]. The key message here is that vastly different methods are found under the umbrella term "Ragone plots".

3.3.2. Model-based

Model-based derivation of Ragone plots is principally conducted following the same procedure as the experimental method detailed in Section 3.3.1:
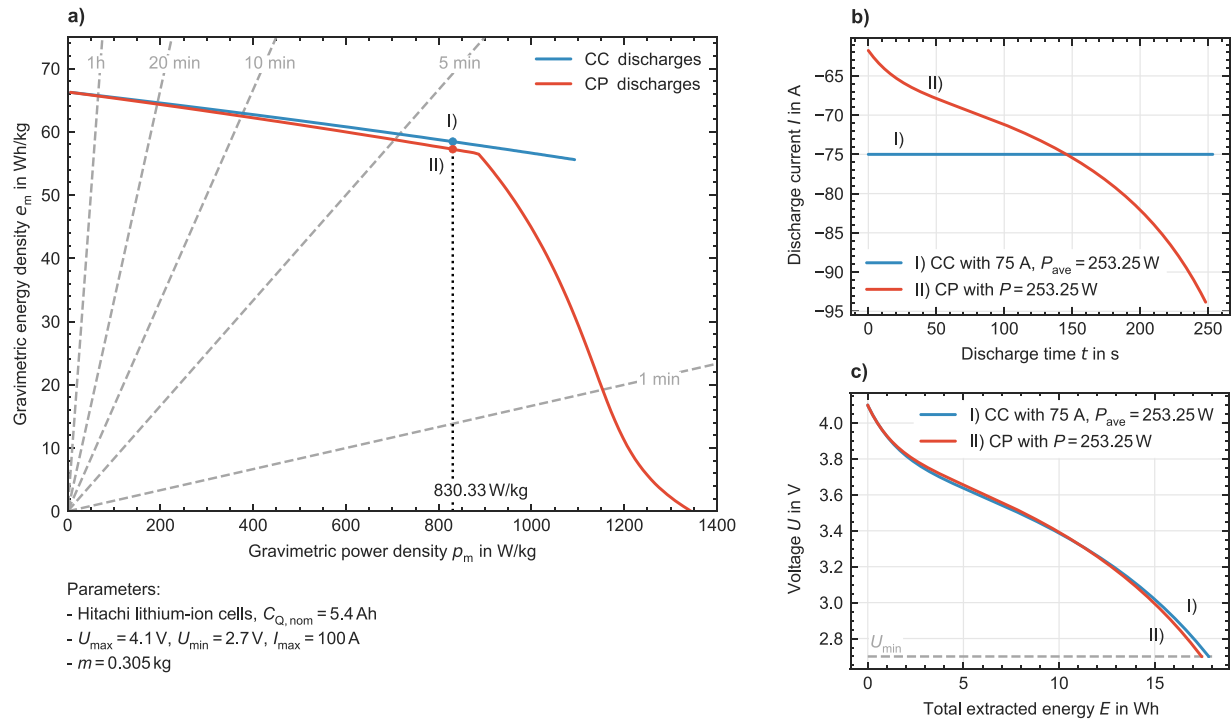
Fig. 5. Subfigure (a) shows Ragone plots composed of multiple CP discharges (red curve) and CC discharges (blue curve), obtained via simulation from the model described in [73] (further discussed in). The resulting curves confirm that CC discharge results in higher energy densities, particularly at higher power levels, where CP discharges are cut off earlier due to reaching I_{max}. To explain the difference in energy densities, (b) shows the time curve of two single discharges, marked with a blue dot and labeled I (CC) and marked with a red dot and labeled II (CP). Both these single discharges result in the same (average) power density (830.33 W/kg), as shown with the dotted vertical line in (a). Subfigure (b) shows that the high currents at the end of the CP discharge process result in higher polarization, and as a result, the minimum voltage U_{min} is reached earlier, see (c). This results in less energy extracted (Peukert's law), as shown on the x-axis of (c). (For interpretation of the references to color in this figure legend, the reader is referred to the web version of this article.)

1. Formulation of a model that depicts the operating behavior of an energy storage material, device or system.
2. The model is simulated over continuous time at different discharge powers until an operating limit is reached and the process is terminated.
3. Integration of power over time to obtain energy.
4. Each simulation results in an energy–power value pair. All the E-P values together constitute the Ragone curve.

A large variety of models are utilized for this purpose, ranging from simple to complex, from lumped to 2D, and from physical to empirical. A deciding factor in the modeling approach is whether the Ragone plot is the final goal or a byproduct of a general analysis. A Ragone curve describes the E-P relation and, thus, the operating behavior at the terminal of the energy storage. If this is the only goal, the model can be simple and phenomenological as long as the E-P terminal behavior is represented with sufficient accuracy. If the internal operating behavior of a storage technology is of interest, a more physically meaningful, complex model might be chosen, and a Ragone plot produced, among other analyses.

The model requirements can be broadly summarized as follows: the model must be dynamic, at the least in the timescales relevant for the discharge process of the specific technology, because the potential of most energy technologies changes during a discharge. This results in a non-stationary process. The dynamic model formulation is achieved by constituting differential equations, often a balance equation (i.e., mass balance, energy balance, charge balance). Effects outside the discharge timescale can be disregarded if desired or approximated via stationary or quasi-stationary relations. The model formulation must include operating limits that terminate the discharge simulation.

In some cases, typically simpler model formulations, the model can be solved analytically to obtain a closed-form expression that directly gives the energy as a function of power $E(P)$. By eliminating the
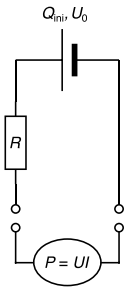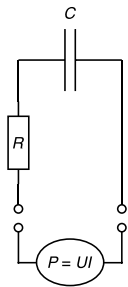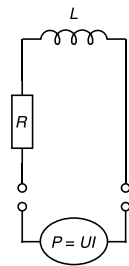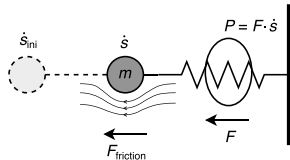
temporal component, simulation over time is not required and the evaluation of $E(P)$ for different discharge powers results directly in the Ragone curve.

We omit further sub-distinctions between model-based Ragone plots in the introduced taxonomy; see Table 1. While there is a certain clustering into groups of similar approaches in the literature, a clear separation is difficult. A particular model-based approach to characterize batteries could combine, e.g., elements of porous electrode theory with equivalent circuit models. Envisioning all possible modeling approaches and creating placeholder classifiers in a taxonomy is also difficult. In effect, any approach that meets the abovementioned requirements and models the operating behavior at the storage terminals as accurately as necessary can be used. However, to give the discussion of model-based Ragone plots some structure, we discuss selected modeling approach groupings that have high relevance in the context of Ragone plots in the order they were first applied in the field. Note that there is a bias towards electrochemical energy storage because the Ragone plot historically originates from this field.

Porous electrode theory (Doyle–Fuller–Newman model family). The Doyle–Fuller–Newman (DFN) battery model and its subsequent extensions and advancements is a popular full-cell formulation for intercalation systems, such as lithium-ion batteries [76]. It is a pseudo-two-dimensional model based on porous electrode theory, primarily derived from fundamental theory. It is a state-of-the-art, physics-based model [77], but it comes at the cost of a complex implementation and computationally expensive simulation. Due to the model complexity, it is disproportionate as a standalone ansatz for obtaining Ragone curves, where simpler models suffice. Instead, DFN-implementations have been used for producing Ragone curves as one element of broader model-based analyses.

Doyle et al. [68] investigate the design optimization of lithium-polymer cells to increase energy density, whereby the optimization

Table 2
Overview over the storage technologies described by Christen and Carlen 2000 and Christen 2018.
Source: Graphical representations adapted from [9,28].

General battery	Capacitor	SMES	Flywheel
no inductive element, $V(Q) = U_0$	no inductive element, $V(Q) = Q/C$	no potential term	no potential term
$-R \cdot I + U_0 = U$	$-R \cdot I + \dfrac{Q}{C} = U$	$L \cdot \dot{I} - R \cdot I = U$	$m \cdot \ddot{s} + \dfrac{m}{\tau} \cdot \dot{s} = F$

result is assessed via Ragone plots. Similar DFN-based design optimizations with Ragone plots for various lithium-ion chemistries have been conducted by [78–81]. The DFN model has also been employed to model pulsed discharge Ragone plots by Stewart et al. [82]. In this case, the DFN model can accurately model the electrolyte dynamics that occur in a pulsed discharge, i.e., the concentration polarization during the pulse and the subsequent voltage recovery in the idle time.

"Theory of Ragone plots" by Christen and Carlen. This dedicated Ragone plot ansatz was put forward by Christen and Carlen in 2000 [9] and elaborated and expanded upon in [28]. It consists of a compact set of differential equations (one for each technology), solved analytically to produce an expression of $E(P)$. The original publication contributed significantly to popularizing the Ragone plot.

At the heart lies the formulation of two general differential equations with the same structure, see Eqs. (8) and (9). The first describes the dynamics of an ideal electrical energy storage with the charge Q, containing an inductance L, an internal resistance R, a potential $V(Q)$ and delivering a voltage U to the load. The other considers an ideal mechanical energy storage, where a point mass with the coordinate s and mass m moves in a potential ψ, is slowed down by a Stokes-type friction with the time constant τ and delivers a force F to the load.

$$L\frac{\mathrm{d}^2 Q}{\mathrm{d}t^2} + R\frac{\mathrm{d}Q}{\mathrm{d}t} + V(Q) = U \quad \text{with} \quad -\frac{\mathrm{d}Q}{\mathrm{d}t} = I \tag{8}$$

$$m\frac{\mathrm{d}^2 s}{\mathrm{d}t^2} + \frac{m}{\tau}\frac{\mathrm{d}s}{\mathrm{d}t} + \psi(s) = F \quad \text{with} \quad \frac{\mathrm{d}s}{\mathrm{d}t} = \dot{s} \tag{9}$$

The general equations are then modified to fit the specific technologies. For example, the battery has no inductive element, and the potential $V(Q)$ is substituted by a constant voltage U_0. In the case of a supercapacitor, which also has no inductive element, the potential $V(Q)$ is given by Q/C. The superconducting magnetic energy (SMES) and flywheel storage have no potential term. An overview of the technology-specific equations that result from these modifications and their equivalent circuit/graphical representations are given in Table 2. A fifth technology (mechanical potential energy storage, such as pumped hydro) is discussed in principle but not formally developed.

The equations in Table 2 are then solved analytically, and $E(P)$ is determined with algebraic manipulation. For batteries, the Ragone curve is given in Eq. (10); for the other $E(P)$ equations, refer to [9,28]. The relation in Eq. (10) has resurfaced in different forms in other publications. The "modified Ragone representation" of [83] and [84]

is essentially the same mathematical relation with a slightly different notation. The analytical relation in the form $P(E)$ presented by [58] also delivers the same values as Eq. (10).

$$E(P) = \frac{2RQ_0 P}{U_0 - \sqrt{U_0^2 - 4RP}} \tag{10}$$
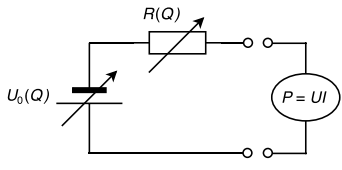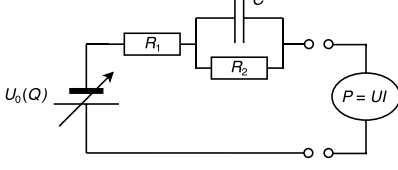
There are several simplifications in this ideal-component approach taken by Christen and Carlen. Most crucial for batteries, no voltage limits are enforced, and the source voltage has no charge-dependency. Krieger and Arnold [85] show that this causes significant discrepancies to experimental results of real batteries and have proposed modifications to the equations of Christen and Carlen. Donateo and Spedicato [86] and Reichbach et al. [87] have proposed other extensions. As for capacitors, a constant capacitance simplifies actual supercapacitor behavior, where C is a function of Q due to pseudocapacitance. Indeed, Mathis et al. [63] argue against using any constant-capacitance formulas to obtain energy values of real supercapacitors. For flywheels, the E-P relation does not account for an attached conversion device, i.e., the motor/generator, that limits the power transfer to the load [28].

Overall, the $E(P)$ relations obtained from this ansatz are easy to use and parametrize from basic experiments or even datasheet information when no experimental resources are available. It is an elegant formulation that serves as a solid foundation for the Ragone plot framework and has excellent teaching value. However, the theoretical nature and limitations this entails reduce the applicability for practical energy storage problems.

Equivalent circuit models. While the approach of Christen and Carlen in the previous subsection also contains simple equivalent circuit representations, equivalent circuit models (ECMs) of higher complexity are often chosen as a dedicated modeling ansatz for quantifying the energy–power relation of electrochemical energy storage, such as batteries and supercapacitors.

The basic principle is based on the phenomenological representation of real-life electrochemical storage operating behavior through an equivalent electric circuit. The equivalent circuit models benefit from a typically lower parameter set and thus a high computational speed [77]. They also have a high degree of flexibility. They can be adapted and expanded to suit modeling demands, e.g., different time constants of parallel RC-elements can represent dynamic

Table 3

Suitable equivalent circuit models for lithium-ion battery Ragone plots. Formulae for Thevenin-circuit from [73].

Rint-circuit	Thevenin-circuit

$$U = U_0(Q) - R(Q, I) \cdot I$$

$$U_{\min} \leq U \leq U_{\max}$$
$$Q(t = 0) = Q_{\text{ini}}$$
$$-\mathrm{d}Q / \mathrm{d}t = I$$
$$I \leq I_{\max}$$

$$R_1 \frac{\mathrm{d}I}{\mathrm{d}t} + \frac{1}{C}\left(1 + \frac{R_1}{R_2}\right) I = \frac{\mathrm{d}U}{\mathrm{d}t} + \frac{1}{R_2 C}(U - U_0(Q))$$

$$U_{\min} \leq U \leq U_{\max}$$
$$Q(t = 0) = Q_{\text{ini}}$$
$$-\mathrm{d}Q / \mathrm{d}t = I$$
$$I \leq I_{\max}$$

behavior in different timescales [88]. While more sophisticated circuits generally increase model accuracy [89], more elements increase the parametrization effort and simulation time. Furthermore, as phenomenological models, ECMs are, strictly speaking, valid only within their parametrization range, and any extrapolation should be treated with caution.

Two lithium-ion battery ECMs that have been employed for obtaining Ragone plots and proven themselves very suitable are the so-called "Rint-circuit" and "Thevenin-circuit". They are presented in Table 3 with their key equations. We limit the discussion to these two examples, as, in theory, ECMs of all shapes and sizes could be used to obtain Ragone plots of any electrochemical cells. Extensive reviews on ECMs employed in battery and supercapacitor modeling have been done elsewhere; see [89,90].

The Rint-ECM contains a voltage source (open-circuit voltage) with a series resistance, representing the cell's internal resistance. The Rint-ECM is the same circuit architecture used by Christen and Carlen in their "Theory of Ragone plots". However, for practical characterization with the Rint-ECM, the open-circuit voltage is typically implemented as charge-dependent and the internal resistance as both charge and current-dependent. These are fitted in polynomial form from experimental data, e.g., in [69,73,85]. $U_0(Q)$ and $R(Q, I)$ are key factors for the good agreement of the relatively simple model architecture, but also why the model needs to be solved numerically. An analytical solution cannot be found with an open-circuit voltage polynomial. Zhang et al. [69] coupled a Rint-model with a thermodynamic model to develop non-isothermal Ragone plots for popular commercial lithium-ion cells. They demonstrate the good agreement of a Rint-circuit with experimental Ragone plots. While they do not test the accuracy at high discharge powers, in general, Rint-model accuracy is lower at higher powers ($\leq 5\%$ error at high currents compared to only $\leq 1\%$ error at low currents, according to [91]).

The Thevenin-circuit is a structurally more complex ECM. In addition to an experimentally fitted voltage source (open-circuit voltage) and an internal series resistance for ohmic-type losses, it contains a parallel resistor–capacitor element. The parallel resistor–capacitor represents the time-dependent charge depletion and recovery at the battery electrodes (the double layer behavior) [92]. Verbrugge and Ying [73] parametrized a Thevenin-ECM to produce lithium-ion battery Ragone plots for a wide temperature range and showed good agreement with experimental results. The experiments do not cover the high power density range, but Thevenin-models are principally suited for this. They are especially suited for pulsed-discharge Ragone plots because the RC-element models the voltage recovery in idle time, where Rint-models would be unsuitable.

Because equivalent circuit models are phenomenological, they cannot give information about the behavior of internal physical variables. However, if the end goal is only to create a Ragone plot, this is not a drawback but rather a benefit. As mentioned at the outset of this chapter, energy–power relations fundamentally characterize the operating behavior at the terminal of the energy storage. Modeling the exact inner workings is optional as long as the terminal behavior is represented correctly. Here, ECMs offer an excellent trade-off between accuracy and implementation effort.

Endoreversible thermodynamics. To describe the energy–power relations of PTES (also referred to as Carnot batteries), Christen uses endoreversible thermodynamics as a modeling framework in [31]. The motivation behind endoreversible thermodynamics is to formulate simple expressions that better match real-life processes than reversible thermodynamics [93]. This is achieved by considering ideal, reversible subsystems whose interactions with each other are irreversible.

In [31], an ideal Carnot engine which is connected to a lumped thermal reservoir with the thermal capacitance C_{th} and temperature T, that decays during the discharge (sensible TES) or remains constant (latent TES). The heat is transferred to the Carnot engine via an irreversible heat exchanger with an equivalent thermal resistance R_{th}. The differential equation is solved analytically, resulting in a time-independent, normalized $E(P)$ relation. The fundamental E-P curve can thus quickly be obtained from the lumped parameters C_{th} and R_{th}. However, due to the uncertainty of the lumped parameters and the relative simplicity of the model, the Ragone curves of practical technical systems could differ, as control regimes and off-design performance of power cycle machinery pose significant challenges for PTES.

3.3.3. Datasheet-based

Datasheet-based or datasheet-enhanced methods to obtain Ragone curves can be helpful when experimental infrastructure is unavailable, and a quick solution is preferred. Mellincovsky et al. [94] and Reichbach et al. [87] have proposed datasheet-enhanced methods to obtain Ragone curves, where the modeling approach is fed by parameters readily available from commercial supercapacitor datasheets.

Chen et al. [95] proposed a method whereby the entire Ragone curve is derived from experimental datasheet discharges performed by the manufacturer of commercial battery cells. Here, at least two voltage-capacity curves for different discharge currents are required. Two energy-discharge time value pairs can be extracted from these curves, converted to E-P value pairs, and subsequently interpolated. The accuracy thus depends on the number of discharge curves that are processed. This method has also been proposed in a similar form by [46,69].

3.4. Technology

The entries in the taxonomy facet "technology" in Table 1 are all the technologies for which Ragone plots have ever been created. The technologies include various battery types, where the Ragone plot is traditionally applied, and other technologies, such as CAES and PTES. Instead of covering every technology separately, we want to introduce another dimension, namely coupled E-P and decoupled E-P, for the discussion in this chapter. This distinction is not included in the taxonomy because it is an overarching characteristic that groups several technologies, but it helps understand the underlying mechanisms. Section 3.4.1 explains coupled vs. decoupled E-P characteristics and their effect on the Ragone plot. After this, batteries and supercapacitors (coupled E-P) are discussed 3.4.2, then all other technologies (decoupled E-P) in 3.4.3. Lastly, thermal energy storage is discussed separately because it is not electric energy storage but rather a key component in electric energy storage technologies.

3.4.1. Coupled E-P vs. decoupled E-P technologies

Energy storage technologies can be grouped into two categories: coupled E-P type technologies, where energy and power are linked together and decoupled E-P type storage, where energy and power can be scaled separately.

Most storage systems based on electrochemical cells are coupled E-P type technologies (except for flow batteries). Here, designing and optimizing for energy comes at the expense of power and vice versa. For example, a cell can be designed to increase power performance by adding more conductive additives and current collectors. However, within a finite cell volume, this leaves less space for active material and, therefore, comes at the price of energy performance [96,97]. Specific energy and specific power are thus not independent from one another, hence the term "coupled E-P". While the cell's E/P ratio is a design choice within a certain range, they are subsequently mass-produced as a sealed-off component whose E/P ratio cannot be modified. A storage system composed of cells has the same E/P ratio as its constituent cells.

In a decoupled E-P type technology, energy and power can be scaled separately, such as pumped hydro, compressed air energy storage [98], flow batteries or flywheel energy storage [99]. These are storage technologies where the conversion from stored energy form to electrical output is performed by a dedicated device, e.g., motor/generator or turbine/compressor. These are separate from the energy reservoir, and both can be scaled to whichever absolute size is needed; hence the term "decoupled E-P".

Fig. 6 conceptually illustrates the impact of coupled vs. decoupled E-P on the specific-value Ragone plot. In Fig. 6(a), the Ragone curves of three different example cells are plotted, designed by three different manufacturers, but belonging to the same technology (e.g., a specific battery chemistry). Cell 1 is a high-energy cell, cell 3 is a high-power cell and cell 2 lies between the two. They are limited by a technology-inherent maximum gravimetric energy density $e_{m,max}$. Each cell has its own E-P trade-off *in operation*, characterized by the Ragone curve. However, taken together, their nominal operating points form a Pareto front, characterizing the E-P trade-off *in design*.

Tzermias et al. [39] first practically demonstrated this Pareto front by plotting many nominal energy and power densities of state-of-the-art commercial lithium-ion cells, see Fig. 2(c), further discussed in Section 3.7. In the case of a coupled E-P type technology, a specific-value Ragone plot can aid in honest reporting because a cell claiming superior power performance will have a worse energy performance in a finite volume/mass.

Fig. 6(b) shows three example systems of a decoupled E-P type technology. The technology is characterized by an inherent $e_{m,max}$, largely determined by the storage medium (e.g., air/water/hydrogen). The power conversion units typically take up less volume and mass in relation to the energy reservoir and, therefore, do not impact energy density substantially. Decoupled E-P technologies thus have a

Electrochemical ES technology	Ragone plot literature
Lithium-ion batteries (LIB)	Nagasubramanian 2001 [101]
	Chu and Braatz 2002 [102]
	Zhang et al. 2006 (LCO) [103]
	Verbrugge and Ying [73]
	Moss et al. 2008 (Lipo) [104]
	Ji et al. 2012 (NMC) [105]
	Krieger and Arnold 2012 [85]
	Kumar et al. 2018 (LCO) [106]
	Sarpal et al. 2018 [46]
	Braun et al. 2018 (ASS) [107]
	Zhang et al. 2019 (NCA, NMC) [69]
	Schröer et al. 2020 (LTO) [59]
	Catenaro et al. 2021 (NCA, NMC, LFP) [58]
Lead–acid batteries (LAB)	Saakes et al. 2001 [108]
	Lopes et al. 2011 [36]
	Zhang et al. 2015 [37]
Nickel-metal-hydride (NMH)	Schupbach et al. 2003 [35]
	Albertus et al. 2008 [80]
	Ceralo et al. 2020 [109]
Lithium-sulphur batteries (LSB)	Mikhaylik and Akridge 2003 [110]
	Akridge et al. 2004 [111]
Supercapacitors (SC)	Chu and Braatz 2002 [102]
	Moss et al. 2007 [112]
	Cericola et al. 2010 [54]
	Lopes et al. 2011 [36]
	Reichbach et al. 2016 [87]
	Allagui et al. 2020 [72]
	Catenaro et al. 2021 [58]
Hybrid energy storage (HESS) of LIB and SC	Holland et al. 2002 [51]
	Sikha and Popov 2004 [52]
	Sikha et al. 2005 [53]

characteristic energy density, but the power density can be scaled independently, as needed. However, their Ragone curves still show operating behavior E-P trade-off, as operation at different powers results in different available energies. As such, they have other benefits, discussed in Section 3.4.3.

3.4.2. Batteries and supercapacitors (coupled E-P)

Historically, the Ragone plot has been developed for characterizing batteries and supercapacitors as coupled E-P type storage technologies. Ragone plot analysis has proven itself especially suitable here because energy and power densities are key characteristics for mobile applications [100], where energy storage is unavoidable, and new chemistries are typically established first.

The Ragone curve shape of batteries and supercapacitors is characterized by very low leakages in practically relevant charge/discharge timeframes. The highest available energy is in the low power range and continually decreases as the discharge power increases. In the high-power region, the available energy drops rapidly due to the ohmic losses associated with high currents and polarization effects.

Over the last years, a continual development towards higher energy and power densities has been reflected in Ragone plots, in line with overarching battery development trends. This development will not be discussed in detail, as the Ragone plot is merely the reporting framework and battery development trends are reviewed in detail elsewhere. For an overview of past and recent cell-level battery and supercapacitor characterizations via Ragone plots, refer to Table 4.

3.4.3. Other technologies (decoupled E-P)

Ragone plots are not typically used for decoupled E-P-type technologies. One reason is that decoupled E-P is primarily implemented as stationary storage, where energy and power density are less relevant. Another factor is research tradition: particular subfields might not be aware of the Ragone plot framework or question the application to
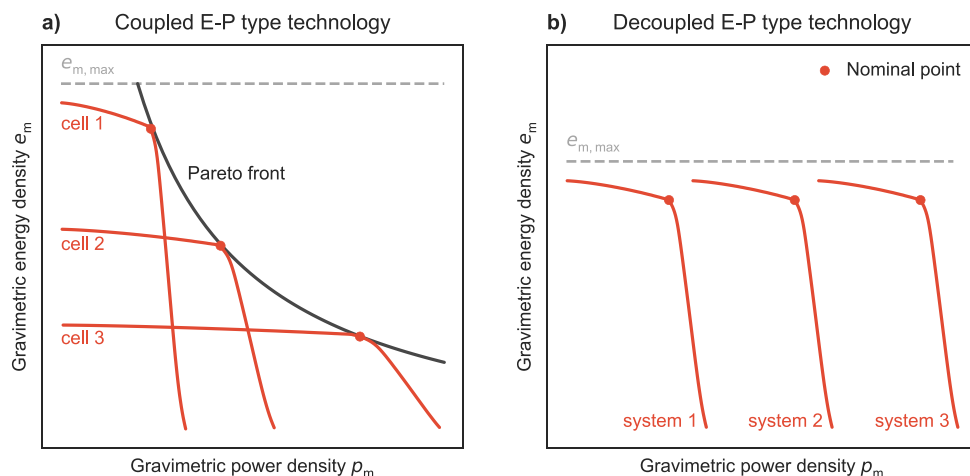
Fig. 6. Depiction of the conceptual difference between specific-value Ragone plots of coupled and decoupled E-P technology types. Decoupled E-P type Ragone curves only quantify the E-P trade-off incurred by operation at different power levels.

their respective technologies. Ragone plots have other benefits in cases where energy and power density are less relevant, as discussed in the following subsections.

Redox-flow batteries. While many material-level Ragone plot studies for flow batteries of all kinds can be found, only [113] characterized commercial vanadium redox-flow battery cells with Ragone plots to estimate their potential for integration with wind power. Too few E-P data points are collected to conclude a characteristic shape, but an energy drop at high powers can be seen as with all electrochemical energy storage.

The lack of component (cell) and system-level E-P characterization indicates a general trend in the redox-flow battery community, where the focus lies on material-level research. According to Arenas et al. [114], "there are very few case studies of scale-up, full-size cell characterization or plant performance during extended operation".

Flywheels, Carnot batteries. Christen has presented Ragone plots for flywheel energy storage [28] and for pumped thermal energy storage (PTES), also referred to as Carnot batteries, with both latent and sensible thermal energy storage [31]. In the case of the flywheel energy storage, it is a simplified analysis that does not account for the effects of the motor/generator and is, therefore, not studied in terms of a decoupled E-P technology. The characteristic shape shows the low-power range dominated by leakage losses due to friction, but no equivalent effects to polarization occur at high discharge powers.

In the case of Carnot batteries, the characteristic shape is different for sensible and latent heat reservoirs. In general, the Ragone curve is bounded by the efficiency of the thermodynamic cycle and the available energy is reduced at higher powers due to imperfect heat exchange. Both characterizations are theoretical but are a solid basis for further practical analysis. For details, the reader is referred to the respective publications [28,31].

Compressed air energy storage (CAES). Alami et al. have experimentally characterized both CAES [24] and compressed gas energy storage (CGES) [25] with Ragone plots. The analyses use the same prototypic system, once with air as a working fluid and once with CO_2. The system consists of three pressure cylinders, two reciprocating compressors, a turbine and a motor/generator. While prototypic in nature, it is a true system-level analysis. One issue in the analysis is calculating the power density from the maximum values of the generator voltage and current, which is an overestimation. Nevertheless, the gain from the Ragone representation can be seen in this case, namely (1) a compact display of the general attainable energy and power and density, (2) showing general operating flexibility (range of operating powers) and the associated available energy reduction of off-design behavior and

(3) quantifying the effect of different operating regimes and operating limits on attainable energy and power (and their densities).

3.4.4. Thermal energy storage (TES)

Standalone TES is not an electric energy storage technology, as the input and output are thermal energy. It is, however, a key component for electric storage technologies, such as CAES [115] or Carnot batteries [116], and thus it is briefly discussed here.

Thermal energy storage can be coupled E-P or decoupled E-P, depending on its configuration. In engineering applications, thermal energy is typically transferred to a working fluid via a heat exchanger. This heat exchanger can be integrated into the TES or implemented as a separate component. An example of a coupled E-P type would be a latent TES composed of phase change material (PCM) with an integrated heat exchanger in the form of spatially distributed fluid channels. Inserting more heat exchanger channels allows the thermal energy to be transferred more quickly but reduces the amount of phase change material and, therefore, the energy capacity [30]. In contrast, a decoupled E-P TES has a separate heat exchanger component that can be scaled independently. Increasing power density thus does not come at the expense of energy density.

Recent publications in the field of thermal energy storage have adopted the Ragone plot framework to great effect, see [29,30,117, 118]. The most extensive investigation in this regard is [30]. Here, analogies between electrochemical and thermal energy storage are developed, and Ragone plots are first adapted for TES. Instead of electrical power, the equivalent axis for TES is the heat transfer rate $\dot{q}$. A comprehensive parameter study of PCM-based heat storage design is conducted, and different PCM materials are tested, all in the Ragone plot framework.

Because it clearly shows the effect of design variables on power and energy density, the Ragone plot is a compact way to investigate design trade-offs at the initial design stage on the same basis scenario. At the same time, by including both energy (density) and power (density), disingenuous performance reporting is prevented [30]. It remains to be seen if the Ragone plot framework prevails in TES performance reporting, but it is fundamentally well-suited for this.

3.5. Process direction

All the Ragone plots discussed thus far showed discharge processes, as most of the Ragone plot literature focuses on the discharge direction. A guess as to why this is the case is that many energy storage applications are more discharge-constrained, e.g., electric vehicles charged
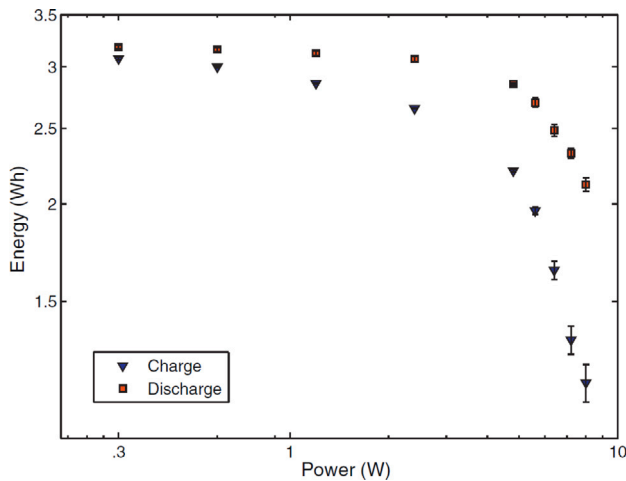
Fig. 7. Experimental Ragone curves for the charge and discharge direction of commercial lithium-ion cells (900 mAh, Tenergy). Used with permission of Elsevier Science & Technology Journals, from [85] with minor edits; permission conveyed through Copyright Clearance Center, Inc.

slowly overnight but discharged with high-power, dynamic load demands. However, the Ragone plot concept equally applies to the charge process direction.

Two notable publications that include the charge and discharge directions are [73] and [85]. Both studied commercial lithium-ion cells via equivalent circuit models and CP charge and discharge. Both highlight the different operating behavior and the resulting different Ragone plots for the charge and discharge direction. This effect is due to the well-known voltage hysteresis that occurs in lithium-ion batteries [119].

The result from [85] is shown in Fig. 7, where the charge direction Ragone curve is lower than the discharge curve because the tested cells are optimized for discharge. Charge and discharge are not symmetrical processes, and a Ragone plot for the charge direction is, therefore, not a mirrored discharge Ragone plot. Similar effects can be expected from other storage technologies but have not yet been studied with the Ragone plot framework.

3.6. Visualization

The visualization of Ragone plots is highly variable, and no form of presentation has established itself above others (see supplementary materials, Appendix). From the literature review, four classification aspects have been identified: which values are displayed, the axis orientation, whether values are normalized or not, and the usage of logarithmic axes. However, these four aspects are not deemed sufficiently important to merit their own taxonomy facet and thus have been grouped under the facet "visualization", discussed briefly in this subsection.

First, energy and power can be displayed as absolute values or as derived specific values based on mass (gravimetric) or volume (volumetric). This choice depends entirely on the context and utilization of the Ragone plot.

Second, the axes of the diagram can either be oriented as energy over power (or the derived specific quantities) or vice-versa. As with other visualization options, the literature has no dominant axis orientation. However, a recommendation is made here: We consider plotting the energy on the *y*-axis as a function of applied power (on the *x*-axis) a more intuitive axis choice. Adopting this as a guideline would ensure a standard orientation of all Ragone plots, which is beneficial for easy comparison between plots.

Third, the quantities in the Ragone plot can be normalized to a reference value, typically either the maximum or the nominal value.

Normalization is helpful when comparing energy storage in cases where mass and volume are irrelevant to the application, but some reference point is needed. As with the choice between absolute and specific values, this depends on the context.

Finally, the axes' scaling can be either logarithmic, linear or semilogarithmic with respect to energy or power. Logarithmic visualization is beneficial when multiple technologies are included in the same Ragone plot, as it facilitates the display of different orders of magnitude of E, P or derived specific quantities within one diagram. If this is not the case, logarithmic visualization should be applied sparingly, as it visually distorts the characteristic shape of the Ragone curve.

In all cases, it is good practice to include isochrones so that the range of the Ragone curve can be quickly gauged and compared between different plots.

3.7. Utilization

The primary purpose of a Ragone plot is to visualize the relationship between energy and power and thus facilitate the comparison between different types of energy storage, which is discussed in Section 3.7.1. However, other utilization beyond this primary purpose is possible, broadly grouped into two further classifiers, namely the inclusion into optimization problems as a constraint, discussed in Section 3.7.2 and graphical sizing/design methods in Section 3.7.3.

3.7.1. Visualization & comparison

Different aspects can be visualized and compared via Ragone plots. Firstly, the impact of physical effects on the E-P relation can be shown. Temperature effects in lithium-ion batteries and their influence on Ragone curves are investigated in [103,105,106]. The non-isothermal Ragone plot of Ji et al. [105] demonstrates that self-heating results in higher specific energies but an even more accentuated final energy drop, referred to as "power cliff". The effect of aging on Ragone plots of lithium-ion batteries is shown in [120], where the Ragone curve is offset towards lower energies with increased aging.

Second, the effect of different design choice parameters can be shown. This effect is often shown in cell design, where the cell architecture is optimized for a specific discharge duration. The Ragone plot is not formally integrated into this parametric optimization process but is used to evaluate the intermediate and final optimization result, see, e.g., [68,78,79,81,121,122].

Third, a technology selection or pre-selection can take place. In [41], a structured technology pre-selection for the supply of pulsed loads of an all-electric warship is conducted via a Ragone plot. Lastly, goal values can be included to assess suitability for an application goal or to show the gap between state-of-art and a specific development goal, e.g., [80].

3.7.2. Optimization constraint

The E-P relation can also be integrated into optimization problems as a mathematical constraint. This approach is often used in hybrid energy storage (HESS), where two storage types with different specific energies/powers are combined. Schupbach et al. [35] introduce the principal procedure. In its simplest form, a single E_{demand} and P_{demand} are supplied by combining storage *a* with storage *b*. The problem constraints are then

$$P_{demand} \leq p_{m,a} \cdot m_a + p_{m,b} \cdot m_b \tag{11}$$

$$E_{demand} \leq e_{m,a}(p_{m,a}) \cdot m_a + e_{m,b}(p_{m,b}) \cdot m_b, \tag{12}$$

where $e_m(p_m)$ are the specific-value Ragone curves. The simplest objective function is a mass minimization, i.e,

$$min(m_a + m_b) \tag{13}$$

The sophistication can be augmented with more complex objective functions or a time-varying power demand, in which case the control
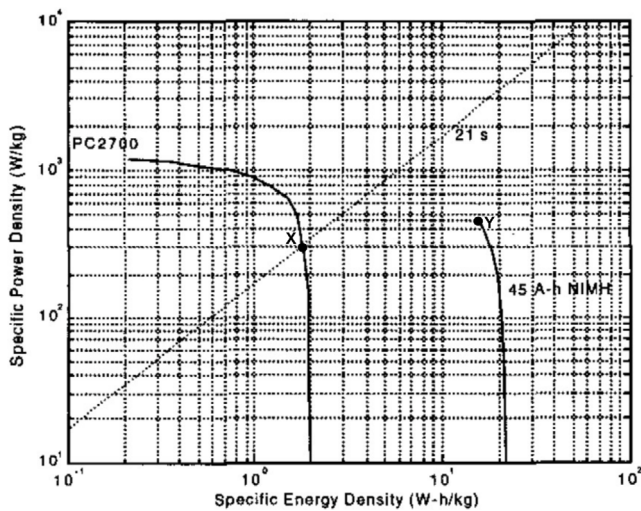
Fig. 8. Ragone plot for a PC2700 Maxwell supercapacitor and an 45 Ah NMH Ovonic battery with graphical sizing method.
Source: Reprinted, with permission, from [35] with minor edits.
© 2003 IEEE.

Fig. 9. Ragone plot analysis method of [39], Figure licensed under CC BY 4.0. The SESS line indicates the maximum achievable specific values that can be attained with a single type of cells. By combining high-power and high-energy cells in hybrid energy storage (HESS), tailored specific-value points in the green area can be achieved, resulting in a weight-saving in comparison to an otherwise oversized single cell-type storage. (For interpretation of the references to color in this figure legend, the reader is referred to the web version of this article.)

strategy for power allocation within HESS substantially influences sizing [35]. This principal procedure has also been applied in subsequent literature, e.g., [36,37,123]. Both Lopes et al. [36] and Zhang et al. [37] size a HESS composed of lead–acid batteries and supercapacitors with Ragone-curve constraints. In [36], the required power P_{demand} is the average value of a load profile, whereas [37] and [35] choose the maximum E and P as their characteristic requirement. The latter is more suited for sizing. Additionally, [37] minimizes purchasing costs instead of only system mass.

In [124], Christen and Ohler integrate Ragone curves as constraints into a techno-economic optimization that maximizes the net present value of a storage system to find the optimal operating point in a simplified economic scenario. The objective function is maximized via mathematical differentiation, which has the advantage that the solution is determined analytically without the need for optimization solvers.

3.7.3. Graphical sizing methods

Ragone plots have also been used for graphical sizing and design. Here, the foundation was also laid by [35]. The method is shown in Fig. 8, where supercapacitors and nickel-metal-hydride (NMH) batteries are options for a storage problem.

From the energy E_{demand} and power P_{demand} requirement of the application, a characteristic time can be calculated and plotted as a diagonal isochrone in the E-P plane. The isochrone intersects the specific-value Ragone curve of the supercapacitor in design point X. From either e_{m} or p_{m} at point X, the storage mass $m = P_{\text{demand}}/p_{\text{m}}(\text{X})$ or $m = E_{\text{demand}}/e_{\text{m}}(\text{X})$ and number of cells $n_{\text{cell}} \geq m/m_{\text{cell}}$ is calculated.

The isochrone does not intersect the Ragone curve of the NMH battery in Fig. 8. This does not mean the technology cannot fulfill the absolute E and P requirements — instead, the design point Y closest to the isochrone is chosen for system sizing. The scale-up from a non-intersected point on the Ragone curve results in oversizing with respect to either energy or power. In this case, the resulting NMH battery has a higher E than demanded by the application, as both energy and power requirements need to be fulfilled simultaneously:

$$m \geq P_{\text{demand}}/p_{\text{m}}(\text{Y}) \quad \wedge \quad m \geq E_{\text{demand}}/e_{\text{m}}(\text{Y}) \tag{14}$$

Catenaro et al. also employ this method for technology selection and subsequent sizing of storage systems for electrified military vehicles in [42]. In contrast to [36,37], the analysis by Catenaro et al. employs
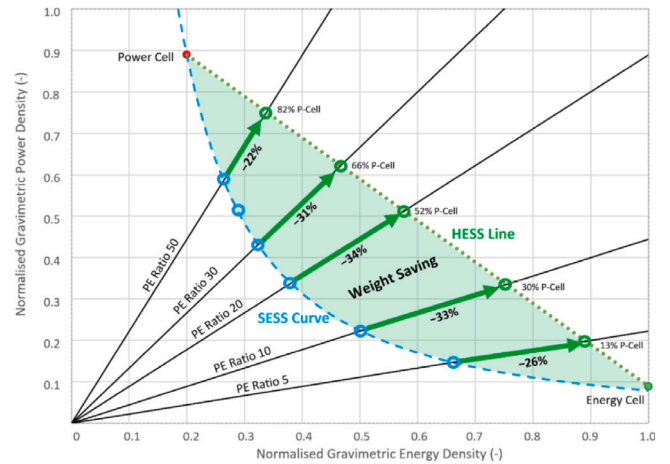
a sophisticated method for calculating the required E_{demand} and P_{demand} for multiple representative vehicle scenarios.

Another interesting graphical method, named the "Ragone plot analysis method", was introduced by Tzermias et al. in [39] for the initial sizing of HESS. By plotting only the nominal power and nominal energy value-pairs of commercially available, state-of-the-art lithium-ion cells shown in Fig. 2(c), the authors quantify the Pareto front of lithium-ion cells as a coupled E-P type technology. This Pareto front is shown in Fig. 9 without the individual cell E-P value pairs and labeled SESS curve (single energy storage system).

A hybrid storage system, combining the cell with the highest gravimetric energy density with the cell that has the highest gravimetric power density, can go beyond the Pareto front and achieve tailored specific-value pairs in the green area in Fig. 9. The outer possible limit is the direct line between the high-power and high-energy cell, labeled HESS line in Fig. 9. The weight-saving potential, in comparison to an otherwise oversized single-cell storage system, can be estimated graphically by the relative length of the distance between the SESS curve and the HESS line in relation to the distance from the origin to the HESS line (for a particular E/P ratio). Exemplary weight savings are quantified with green arrows in Fig. 9. This intuitive and elegant concept allows the user to quickly estimate the weight-saving potential of multi-cell HESS for a particular characteristic $E_{\text{demand}}/P_{\text{demand}}$ ratio. De Freitas et al. [38] proposed a similar concept; however the basis of current cell chemistries renders [39] a more directly practical method.

4. Conclusion and outlook

This work conducted a structured review of the Ragone plot concept. We found that there is not a single understanding of this concept, but rather, a high level of variety and ambiguity characterizes the existing literature. A faceted taxonomy was developed to organize the Ragone plot concept. With the aid of this taxonomy, all relevant aspects of any Ragone plot can be conclusively classified. The authors would like to encourage researchers to classify future Ragone plots using the suggested taxonomy to establish comparability and a shared understanding of this framework. In this work, more than 100 publications have been systematically reviewed via the taxonomy facets. The key findings are summarized in the following subsections.

4.1. Current application

The application of Ragone plots is common in electrochemical energy storage because it historically originates from this field. It is particularly prevalent for material-level analysis, where many novel electrode chemistries are routinely characterized with Ragone plots. Here, the focus lies on potential successors of conventional lithium-ion batteries, such as lithium-metal, lithium-sulfur and solid-state batteries. Furthermore, a blurring of lines between batteries and supercapacitors is occurring, reflected by many material-level HESS analyses. Ragone plots have been used outside of batteries and supercapacitors to great effect; however, these are mainly singular instances, and the framework has yet to establish itself widely. The first adoption of Ragone plots for thermal energy storage has been recorded, where it helps quantify the energy–power trade-off in a finite storage volume.

4.2. Best practices

Several "best practices" for Ragone plots were identified during the review and suggested for future characterization. Generally, a Ragone plot should have an energy axis and a power axis or derived specific quantities of the two. "Proxies" for the energy axis, such as discharge time and efficiency, should not be labeled as Ragone plots, mainly because $\eta(P) \neq E(P)$ in case of residual energy due to, e.g., polarization effects. An axis orientation with energy over power is deemed more intuitive. Practical Ragone curves should comprise multiple E-P value pairs, each obtained by separate, full charge/discharge processes, to predetermined upper/lower operating limits, as described in Section 3.3.1. Adhering to this fundamental principle enables comparison between Ragone curves, even when specific implementations vary in their method (e.g., experimental or via model) or presentation. Operating limits shape the Ragone curve and are part of the information that must always be specified when communicating Ragone plot results. The mode of discharge (CP/CC) influences the obtained values and should be clearly specified. The authors encourage CP tests, which are more relevant in a load-following context. Extrapolation from material-level performance to component-level performance must be transparently communicated and ideally follow guidelines developed in the field of the respective technology.

4.3. Research gaps and future perspectives

The research gaps and future perspectives of the Ragone plot framework are summarized in the following key points:

- **The Ragone plot is not routinely established in all subfields of electric energy storage**. Ragone plot analysis is under-utilized for technologies where energy and power are separately scalable (decoupled E-P). There is value in Ragone plot analysis for these technologies by characterizing off-design performance in a common framework. The Ragone plot shows the E-P trade-off in operating behavior and general operational range. This becomes increasingly relevant as flexible, off-design operation is necessary within power systems with a high share of renewables.
- **Ragone plot analysis at the system level is lacking**. There are few Ragone plot characterizations at the system level. This phenomenon is not specific to Ragone plots but rather symptomatic of general research trends, where comprehensive, system-level analysis of energy storage systems is not as common. However, knowledge of system-level operating behavior and the accompanying technical operating limits, both for the design point and off-design, is crucial for integrating storage into energy system analysis. Here, Ragone plots can provide a means to compare different storage technologies within a common framework on a technical level.

- **Ragone plots can be used as a standard reporting framework for TES**. TES performance has the same fundamental problem as cell-based electrochemical storage: optimizing for either energy or power within a finite volume comes at the expense of the other. Performance reporting of only energy or power is disingenuous; they must be understood as inherently linked. The pioneering usage of Ragone plots in this context should be expanded upon.
- **The potential of Ragone plots for design methods has not yet been fully exploited**. Various design and optimization methods are based on Ragone plots; however, these are still relatively simple. More sophisticated methods can be developed to fully make use of the potential of Ragone plots. These could include, e.g., variation of operating limits, parameter uncertainties or temperature effects within the storage design process.

Ultimately, the Ragone plot is just one tool in the arsenal of energy storage characterization and comparison, but it is particularly useful. It is a simple scenario for energy storage comparison and characterization on equal terms, independent of the technology type and field-specific performance indicators. It functions as a "common language" for different storage technologies in this context. It offers further versatility when integrated into technology selection, initial sizing problems and further optimization methods.

Declaration of competing interest

The authors declare that they have no known competing financial interests or personal relationships that could have appeared to influence the work reported in this paper.

Data availability

Data will be made available on request

Acknowledgments

Appendix A. Supplementary data

Supplementary material related to this article can be found online at https://doi.org/10.1016/j.est.2023.109097.

References

[1] D.V. Ragone, Review of battery systems for electrically powered vehicles, in: Presented At the Mid-Year Meeting of the Society of Automotive Engineers, 1968, 680453, http://dx.doi.org/10.4271/680453.

[2] J.O. Bockris (Ed.), Electrochemistry of Cleaner Environments, Springer US, Boston, MA, 1972, http://dx.doi.org/10.1007/978-1-4684-1950-4.

[3] J.M. Bozek, An Averaging Battery Model for a Lead–Acid Battery Operating in an Electric Car (No. DOE/NASA/1044-79/5), Prepared for U. S. Department of Energy, 1979.

[4] K. Brandt, A 65 ah rechargeable lithium molybdenum disulfide battery, in: The 1985 Goddard Space Flight Center Battery Workshop, NASA Goddard Space Flight Center, 1985, pp. 131–144.

[5] F. Hornstra, A simple methodology for obtaining battery discharge times (and vehicle ranges) for arbitrarily structured load profiles, J. Power Sources 17 (1986) 284–294, http://dx.doi.org/10.1016/0378-7753(86)80049-0.

[6] Y. Ma, M.M. Doeff, S.J. Visco, L.C. De Jonghe, Rechargeable Na / Na x CoO2 and Na15Pb4 / Na x CoO2 polymer electrolyte cells, J. Electrochem. Soc. 140 (1993) 2726–2733, http://dx.doi.org/10.1149/1.2220900.

[7] F. Bonino, S. Panero, M. Pasquali, G. Pistoia, Rechargeable lithium batteries based on Li1 + xV3O8 thin films, J. Power Sources 56 (1995) 193–196, http://dx.doi.org/10.1016/0378-7753(95)80033-D.

[8] W.G. Pell, B.E. Conway, Quantitative modeling of factors determining Ragone plots for batteries and electrochemical capacitors, J. Power Sources 63 (1996) 255–266, http://dx.doi.org/10.1016/S0378-7753(96)02525-6.

[9] T. Christen, M.W. Carlen, Theory of Ragone plots, J. Power Sources 91 (2000) 210–216, http://dx.doi.org/10.1016/S0378-7753(00)00474-2.

[10] G. Nagasubramanian, R.G. Jungst, D.H. Doughty, Impedance, power, energy, and pulse performance characteristics of small commercial Li-ion cells, J. Power Sources 83 (1999) 193–203, http://dx.doi.org/10.1016/S0378-7753(99)00296-7.

[11] G. Nagasubramanian, Electrical characteristics of 18650 Li-ion cells at low temperatures, J. Appl. Electrochem. 31 (2001) 99–104, http://dx.doi.org/10.1023/A:1004113825283.

[12] R. Kötz, M. Carlen, Principles and applications of electrochemical capacitors, Electrochim. Acta 45 (2000) 2483–2498, http://dx.doi.org/10.1016/S0013-4686(00)00354-6.

[13] A. Schneuwly, R. Gallay, Properties and applications of supercapacitors from the state-of-the-art to future trends, in: Proceeding PCIM, 2000.

[14] A. Balducci, D. Belanger, T. Brousse, J.W. Long, W. Sugimoto, Perspective—A guideline for reporting performance metrics with electrochemical capacitors: From electrode materials to full devices, J. Electrochem. Soc. 164 (2017) A1487–A1488, http://dx.doi.org/10.1149/2.0851707jes.

[15] H. Song, J. Su, C. Wang, The Anion–Cation relay battery prototype, Small Sci. 1 (2021) 2000030, http://dx.doi.org/10.1002/smsc.202000030.

[16] S. Randau, D.A. Weber, O. Kötz, R. Koerver, P. Braun, A. Weber, E. Ivers-Tiffée, T. Adermann, J. Kulisch, W.G. Zeier, F.H. Richter, J. Janek, Benchmarking the performance of all-solid-state lithium batteries, Nat. Energy 5 (2020) 259–270, http://dx.doi.org/10.1038/s41560-020-0565-1.

[17] S. Ponnada, M.S. Kiai, R. Krishnapriya, R. Singhal, R.K. Sharma, Lithium-free batteries: Needs and challenges, Energy Fuels 36 (2022) 6013–6026, http://dx.doi.org/10.1021/acs.energyfuels.2c00569.

[18] J.Y. Hwang, M. Li, M.F. El-Kady, R.B. Kaner, Next-generation activated carbon supercapacitors: A simple step in electrode processing leads to remarkable gains in energy density, Adv. Funct. Mater. 27 (2017) 1605745, http://dx.doi.org/10.1002/adfm.201605745.

[19] G.A. Tafete, M.K. Abera, G. Thothadri, Review on nanocellulose-based materials for supercapacitors applications, J. Energy Storage 48 (2022) 103938, http://dx.doi.org/10.1016/j.est.2021.103938.

[20] N.S. Shaikh, S.B. Ubale, V.J. Mane, Jasmin S. Shaikh, Vaibhav C. Lokhande, S. Praserthdam, C.D. Lokhande, P. Kanjanaboos, Novel electrodes for supercapacitor: Conducting polymers, metal oxides, chalcogenides, carbides, nitrides, MXenes, and their composites with graphene, J. Alloys Compd. 893 (2022) 161998, http://dx.doi.org/10.1016/j.jallcom.2021.161998.

[21] Poonam, K. Sharma, A. Arora, S.K. Tripathi, Review of supercapacitors: Materials and devices, J. Energy Storage 21 (2019) 801–825, http://dx.doi.org/10.1016/j.est.2019.01.010.

[22] D.P. Dubal, O. Ayyad, V. Ruiz, P. Gómez-Romero, Hybrid energy storage: the merging of battery and supercapacitor chemistries, Chem. Soc. Rev. 44 (2015) 1777–1790, http://dx.doi.org/10.1039/C4CS00266K.

[23] V. Surendran, A. Lal, M.M. Shaijumon, Mass balancing of hybrid ion capacitor electrodes: A simple and generalized semiempirical approach, ACS Appl. Mater. Interfaces 13 (2021) 52610–52619, http://dx.doi.org/10.1021/acsami.1c14731.

[24] A.H. Alami, K. Aokal, J. Abed, M. Alhemyari, Low pressure, modular compressed air energy storage (CAES) system for wind energy storage applications, Renew. Energy 106 (2017) 201–211, http://dx.doi.org/10.1016/j.renene.2017.01.002.

[25] A.H. Alami, Mechanical energy storage for renewable and sustainable energy resources, in: Advances in Science, Technology & Innovation, Springer International Publishing, Cham, 2020, http://dx.doi.org/10.1007/978-3-030-33788-9.

[26] T. Kadyk, C. Winnefeld, R. Hanke-Rauschenbach, U. Krewer, Analysis and design of fuel cell systems for aviation, Energies 11 (375) (2018) http://dx.doi.org/10.3390/en11020375.

[27] A. Rufer, Energy Storage: Systems and Components, first ed., CRC Press/Taylor & Francis Group, Boca Raton London New York, 2018.

[28] T. Christen, Efficiency and Power in Energy Conversion and Storage: Basic Physical Concepts, first ed., CRC Press/Taylor & Francis Group, Boca Raton, FL, 2018.

[29] K. Yazawa, P.J. Shamberger, T.S. Fisher, Ragone relations for thermal energy storage technologies, Front. Mech. Eng. 5 (29) (2019) http://dx.doi.org/10.3389/fmech.2019.00029.

[30] J. Woods, A. Mahvi, A. Goyal, E. Kozubal, A. Odukomaiya, R. Jackson, Rate capability and Ragone plots for phase change thermal energy storage, Nat. Energy 6 (2021) 295–302, http://dx.doi.org/10.1038/s41560-021-00778-w.

[31] T. Christen, Ragone plots and discharge efficiency-power relations of electric and thermal energy storage devices, J. Energy Storage 27 (2020) 101084, http://dx.doi.org/10.1016/j.est.2019.101084.

[32] S.F.J. Flipsen, Power sources compared: The ultimate truth? J. Power Sources 162 (2006) 927–934, http://dx.doi.org/10.1016/j.jpowsour.2005.07.007.

[33] M. Romer, G.H. Miley, N. Luo, R.J. Gimlin, Ragone plot comparison of radioisotope cells and the direct sodium borohydride/hydrogen peroxide fuel cell with chemical batteries, IEEE Trans. Energy Convers. 23 (2008) 171–178, http://dx.doi.org/10.1109/TEC.2007.914159.

[34] T. Kim, J. Yoon, CDI Ragone plot as a functional tool to evaluate desalination performance in capacitive deionization, RSC Adv. 5 (2015) 1456–1461, http://dx.doi.org/10.1039/C4RA11257A.

[35] R.M. Schupbach, J.C. Balda, M. Zolot, B. Kramer, Design methodology of a combined battery-ultracapacitor energy storage unit for vehicle power management, in: IEEE 34th Annual Conference on Power Electronics Specialist, 2003. PESC '03. Presented At the PESC 2003 - Power Electronics Specialist Conference, IEEE, Acapulco, Mexico, 2003, pp. 88–93, http://dx.doi.org/10.1109/PESC.2003.1218278.

[36] J. Lopes, J.A. Pomilio, P.A.V. Ferreira, Optimal sizing of batteries and ultracapacitors for fuel cell electric vehicles, in: IECON 2011-37th Annual Conference of the IEEE Industrial Electronics Society. Presented At the IECON 2011-37th Annual Conference of IEEE Industrial Electronics, IEEE, Melbourne, Vic, Australia, 2011, pp. 4603–4608, http://dx.doi.org/10.1109/IECON.2011.6120068.

[37] Y. Zhang, X. Tang, Z. Qi, Z. Liu, The Ragone plots guided sizing of hybrid storage system for taming the wind power, Int. J. Electr. Power Energy Syst. 65 (2015) 246–253, http://dx.doi.org/10.1016/j.ijepes.2014.10.006.

[38] C.F. de Freitas, P. Bartholomeus, X. Margueron, P. Le Moigne, Ragone plot-based method for sizing an electric vehicle's battery-battery hybrid energy storage system (HESS), in: 2021 IEEE Vehicle Power and Propulsion Conference (VPPC). Presented At the 2021 IEEE Vehicle Power and Propulsion Conference, VPPC, IEEE, Gijon, Spain, 2021, pp. 1–6, http://dx.doi.org/10.1109/VPPC53923.2021.9699182.

[39] G. Tzermias, S. Akehurst, R. Burke, C. Brace, S. George, J. Bernards, C. Smith, Methodology for the optimisation of battery hybrid energy storage systems for mass and volume using a power-to-energy ratio analysis, Batteries 7 (37) (2021) http://dx.doi.org/10.3390/batteries7020037.

[40] A. Hijazi, E. Bideaux, P. Venet, G. Clerc, Electro-thermal sizing of supercapacitor stack for an electrical bus: Bond graph approach, in: 2015 Tenth International Conference on Ecological Vehicles and Renewable Energies (EVER). Presented At the 2015 Tenth International Conference on Ecological Vehicles and Renewable Energies, EVER, IEEE, Monte Carlo, 2015, pp. 1–8, http://dx.doi.org/10.1109/EVER.2015.7112988.

[41] L.J. Rashkin, J.C. Neely, D.G. Wilson, S.F. Glover, N. Doerry, S. Markle, T.J. McCoy, Energy storage design considerations for an MVDC power system, J. Marine Eng. Technol. 19 (2020) 92–103, http://dx.doi.org/10.1080/20464177.2019.1686329.

[42] E. Catenaro, D.M. Rizzo, S. Onori, Framework for energy storage selection to design the next generation of electrified military vehicles, Energy (2021) http://dx.doi.org/10.1016/j.energy.2021.120695.

[43] H. Hedden, The Accidental Taxonomist, second ed., Information Today, Inc, Medford, New Jersey, 2016.

[44] V. Srinivasan, D. Hafemeister, B. Levi, M. Levine, P. Schwartz, Batteries for vehicular applications, in: AIP Conference Proceedings. Presented At the PHYSICS of SUSTAINABLE ENERGY: Using Energy Efficiently and Producing It Renewably, AIP, Berkeley (California), 2008, pp. 283–296, http://dx.doi.org/10.1063/1.2993726.

[45] S. Ben Elghali, R. Outbib, M. Benbouzid, Selecting and optimal sizing of hybridized energy storage systems for tidal energy integration into power grid, J. Mod. Power Syst. Clean Energy 7 (2019) 113–122, http://dx.doi.org/10.1007/s40565-018-0442-0.

[46] I.S. Sarpal, A. Bensmann, J. Mähliß, D. Hennefeld, R. Hanke-Rauschenbach, Characterisation of batteries with E–P-curves: Quantifying the impact of operating conditions on battery performance, Int. J. Electr. Power Energy Syst. 99 (2018) 722–732, http://dx.doi.org/10.1016/j.ijepes.2018.01.017.

[47] T. Ratniyomchai, S. Hillmansen, P. Tricoli, Recent developments and applications of energy storage devices in electrified railways, IET Electr. Syst. Transp. 4 (2014) 9–20, http://dx.doi.org/10.1049/iet-est.2013.0031.

[48] C.L. Benson, C.L. Magee, On improvement rates for renewable energy technologies: Solar PV, wind turbines, capacitors, and batteries, Renew. Energy 68 (2014) 745–751, http://dx.doi.org/10.1016/j.renene.2014.03.002.

[49] Y. Zhao, C.Y. Zhao, C.N. Markides, H. Wang, W. Li, Medium- and high-temperature latent and thermochemical heat storage using metals and metallic compounds as heat storage media: A technical review, Appl. Energy 280 (2020) 115950, http://dx.doi.org/10.1016/j.apenergy.2020.115950.

[50] C. Heubner, K. Voigt, P. Marcinkowski, S. Reuber, K. Nikolowski, M. Schneider, M. Partsch, A. Michaelis, From active materials to battery cells: A straightforward tool to determine performance metrics and support developments at an application-relevant level, Adv. Energy Mater. 11 (2021) 2102647, http://dx.doi.org/10.1002/aenm.202102647.

[51] C.E. Holland, J.W. Weidner, R.A. Dougal, R.E. White, Experimental characterization of hybrid power systems under pulse current loads, J. Power Sources 109 (2002) 32–37, http://dx.doi.org/10.1016/S0378-7753(02)00044-7.

[52] G. Sikha, B.N. Popov, Performance optimization of a battery–capacitor hybrid system, J. Power Sources 134 (2004) 130–138, http://dx.doi.org/10.1016/j.jpowsour.2004.01.054.

[53] G. Sikha, B.N. Popov, Modeling and application studies of an electrochemical hybrid system, Funct. Mater. Lett. 01 (2008) 155–165, http://dx.doi.org/10.1142/S179360470800023X.

[54] D. Cericola, P.W. Ruch, R. Kötz, P. Novák, A. Wokaun, Simulation of a supercapacitor/Li-ion battery hybrid for pulsed applications, J. Power Sources 195 (2010) 2731–2736, http://dx.doi.org/10.1016/j.jpowsour.2009.10.104.

[55] H. Ji, J. Wu, Z. Cai, J. Liu, D.-H. Kwon, Kim, Hyunchul, A. Urban, J.K. Papp, E. Foley, Y. Tian, M. Balasubramanian, Kim, Haegyeom, R.J. Clément, B.D. McCloskey, W. Yang, G. Ceder, Ultrahigh power and energy density in partially ordered lithium-ion cathode materials, Nat. Energy 5 (2020) 213–221, http://dx.doi.org/10.1038/s41560-020-0573-1.

[56] J.R. Croy, B.R. Long, M. Balasubramanian, A path toward cobalt-free lithium-ion cathodes, J. Power Sources 440 (2019) 227113, http://dx.doi.org/10.1016/j.jpowsour.2019.227113.

[57] D. Schmidt, M. Kamlah, V. Knoblauch, Highly densified NCM-cathodes for high energy Li-ion batteries: Microstructural evolution during densification and its influence on the performance of the electrodes, J. Energy Storage 17 (2018) 213–223, http://dx.doi.org/10.1016/j.est.2018.03.002.

[58] E. Catenaro, D.M. Rizzo, S. Onori, Experimental analysis and analytical modeling of Enhanced-Ragone plot, Appl. Energy 291 (2021) 116473, http://dx.doi.org/10.1016/j.apenergy.2021.116473.

[59] P. Schröer, H. van Faassen, T. Nemeth, M. Kuipers, D.U. Sauer, Challenges in modeling high power lithium titanate oxide cells in battery management systems, J. Energy Storage 28 (2020) 101189, http://dx.doi.org/10.1016/j.est.2019.101189.

[60] D.A. Subramaniyan, Validating expensive simulations with expensive experiments: A Bayesian approach, in: Presented At the ASME V & V Symposium, 2012.

[61] A. Vecchi, Y. Li, Y. Ding, P. Mancarella, A. Sciacovelli, Liquid air energy storage (LAES): A review on technology state-of-the-art, integration pathways and future perspectives, Adv. Appl. Energy 3 (2021) 100047, http://dx.doi.org/10.1016/j.adapen.2021.100047.

[62] O. Dumont, G.F. Frate, A. Pillai, S. Lecompte, M. De paepe, V. Lemort, Carnot battery technology: A state-of-the-art review, J. Energy Storage 32 (2020) 101756, http://dx.doi.org/10.1016/j.est.2020.101756.

[63] T.S. Mathis, N. Kurra, X. Wang, D. Pinto, P. Simon, Y. Gogotsi, Energy storage data reporting in perspective—Guidelines for interpreting the performance of electrochemical energy storage systems, Adv. Energy Mater. 9 (2019) 1902007, http://dx.doi.org/10.1002/aenm.201902007.

[64] J.F. Parker, J.S. Ko, D.R. Rolison, J.W. Long, Translating materials-level performance into device-relevant metrics for zinc-based batteries, Joule 2 (2018) 2519–2527, http://dx.doi.org/10.1016/j.joule.2018.11.007.

[65] Y. Gogotsi, P. Simon, True performance metrics in electrochemical energy storage, Science 334 (2011) 917–918, http://dx.doi.org/10.1126/science.1213003.

[66] J.E. Zuliani, J.N. Caguiat, D.W. Kirk, C.Q. Jia, Considerations for consistent characterization of electrochemical double-layer capacitor performance, J. Power Sources 290 (2015) 136–143, http://dx.doi.org/10.1016/j.jpowsour.2015.04.019.

[67] S. Zhang, N. Pan, Supercapacitors performance evaluation, Adv. Energy Mater. 5 (2015) 1401401, http://dx.doi.org/10.1002/aenm.201401401.

[68] M. Doyle, J. Newman, A.S. Gozdz, C.N. Schmutz, J. Tarascon, Comparison of modeling predictions with experimental data from plastic lithium ion cells, J. Electrochem. Soc. 143 (1996) 1890–1903, http://dx.doi.org/10.1149/1.1836921.

[69] Y.C. Zhang, O. Briat, L. Boulon, J.-Y. Deletage, C. Martin, F. Coccetti, J.-M. Vinassa, Non-isothermal Ragone plots of li-ion cells from datasheet and galvanostatic discharge tests, Appl. Energy 247 (2019) 703–715, http://dx.doi.org/10.1016/j.apenergy.2019.04.027.

[70] W. Lajnef, J.-M. Vinassa, O. Briat, S. Azzopardi, E. Woirgard, Characterization methods and modelling of ultracapacitors for use as peak power sources, J. Power Sources 168 (2007) 553–560, http://dx.doi.org/10.1016/j.jpowsour.2007.02.049.

[71] A. Laheäär, P. Przygocki, Q. Abbas, F. Béguin, Appropriate methods for evaluating the efficiency and capacitive behavior of different types of supercapacitors, Electrochem. Commun. 60 (2015) 21–25, http://dx.doi.org/10.1016/j.elecom.2015.07.022.

[72] A. Allagui, M.E. Fouda, A.S. Elwakil, Communication — The Ragone plot of supercapacitors under different loading conditions, J. Electrochem. Soc. 167 (2020) 020533, http://dx.doi.org/10.1149/1945-7111/ab6bb9.

[73] M.W. Verbrugge, R.Y. Ying, Energy vs power relationship for lithium ion cells over a broad range of temperatures and power densities, J. Electrochem. Soc. 154 (A949) (2007) http://dx.doi.org/10.1149/1.2767410.

[74] INEEL, FreedomCAR Battery Test Manual for Power-Assist Hybrid Electric Vehicles (No. DOE/ID-11069), Prepared for the U. S. Department of Energy, 2003.

[75] S. Beninati, L. Damen, M. Mastragostino, Fast sol–gel synthesis of LiFePO4/C for high power lithium-ion batteries for hybrid electric vehicle application, J. Power Sources 194 (2009) 1094–1098, http://dx.doi.org/10.1016/j.jpowsour.2009.06.035.

[76] M. Doyle, T.F. Fuller, J. Newman, Modeling of galvanostatic charge and discharge of the lithium/polymer/insertion cell, J. Electrochem. Soc. 140 (1993) 1526–1533, http://dx.doi.org/10.1149/1.2221597.

[77] F. Brosa Planella, W. Ai, A.M. Boyce, A. Ghosh, I. Korotkin, S. Sahu, V. Sulzer, R. Timms, T.G. Tranter, M. Zyskin, S.J. Cooper, J.S. Edge, J.M. Foster, M. Marinescu, B. Wu, G. Richardson, A continuum of physics-based lithium-ion battery models reviewed, Prog. Energy 4 (2022) 042003, http://dx.doi.org/10.1088/2516-1083/ac7d31.

[78] V. Srinivasan, J. Newman, Design and optimization of a natural graphite/iron phosphate lithium-ion cell, J. Electrochem. Soc. 151 (A1530) (2004) http://dx.doi.org/10.1149/1.1785013.

[79] J. Christensen, V. Srinivasan, J. Newman, Optimization of lithium titanate electrodes for high-power cells, J. Electrochem. Soc. 153 (A560) (2006) http://dx.doi.org/10.1149/1.2172535.

[80] P. Albertus, J. Christensen, J. Newman, Modeling side reactions and nonisothermal effects in nickel metal-hydride batteries, J. Electrochem. Soc. 155 (A48) (2008) http://dx.doi.org/10.1149/1.2801381.

[81] S. Stewart, P. Albertus, V. Srinivasan, I. Plitz, N. Pereira, G. Amatucci, J. Newman, Optimizing the performance of lithium titanate spinel paired with activated carbon or iron phosphate, J. Electrochem. Soc. 155 (A253) (2008) http://dx.doi.org/10.1149/1.2830552.

[82] S.G. Stewart, V. Srinivasan, J. Newman, Modeling the performance of lithium-ion batteries and capacitors during hybrid-electric-vehicle operation, J. Electrochem. Soc. 155 (A664) (2008) http://dx.doi.org/10.1149/1.2953524.

[83] S. Delalay, Etude systemique pour l'alimentation hybride: application aux systemes intermittents, EPFL, Lausanne, 2013, https://infoscience.epfl.ch/record/187365.

[84] A. Rufer, Energy Storage: Systems and Components, CRC Press, Boca Raton London New York, 2018.

[85] E.M. Krieger, C.B. Arnold, Effects of undercharge and internal loss on the rate dependence of battery charge storage efficiency, J. Power Sources 210 (2012) 286–291, http://dx.doi.org/10.1016/j.jpowsour.2012.03.029.

[86] T. Donateo, L. Spedicato, Fuel economy of hybrid electric flight, Appl. Energy 206 (2017) 723–738, http://dx.doi.org/10.1016/j.apenergy.2017.08.229.

[87] N. Reichbach, M. Mellincovsky, M.M. Peretz, A. Kuperman, Long-term wide-temperature supercapacitor Ragone plot based on manufacturer datasheet, IEEE Trans. Energy Convers. 31 (2016) 404–406, http://dx.doi.org/10.1109/TEC.2015.2479407.

[88] N. Devillers, S. Jemei, M.-C. Péra, D. Bienaimé, F. Gustin, Review of characterization methods for supercapacitor modelling, J. Power Sources 246 (2014) 596–608, http://dx.doi.org/10.1016/j.jpowsour.2013.07.116.

[89] L. Zhang, X. Hu, Z. Wang, F. Sun, D.G. Dorrell, A review of supercapacitor modeling, estimation, and applications: A control/management perspective, Renew. Sustain. Energy Rev. 81 (2018) 1868–1878, http://dx.doi.org/10.1016/j.rser.2017.05.283.

[90] X. Zhang, W. Zhang, G. Lei, A review of Li-ion battery equivalent circuit models, Trans. Electr. Electron. Mater. 17 (2016) 311–316, http://dx.doi.org/10.4313/TEEM.2016.17.6.311.

[91] N. Campagna, V. Castiglia, R. Miceli, R.A. Mastromauro, C. Spataro, M. Trapanese, F. Viola, Battery models for battery powered applications: A comparative study, Energies 13 (4085) (2020) http://dx.doi.org/10.3390/en13164085.

[92] A. Seaman, T.-S. Dao, J. McPhee, A survey of mathematics-based equivalent-circuit and electrochemical battery models for hybrid and electric vehicle simulation, J. Power Sources 256 (2014) 410–423, http://dx.doi.org/10.1016/j.jpowsour.2014.01.057.

[93] K.H. Hoffmann, An introduction to endoreversible thermodynamics, Atti Accad. Pelorit. Pericolanti - Cl. Sci. Fis. Mat. Natur. (2008) 1–18, http://dx.doi.org/10.1478/C1S0801011.

[94] M. Mellincovsky, A. Kuperman, C. Lerman, I. Aharon, N. Reichbach, G. Geula, R. Nakash, Performance assessment of a power loaded supercapacitor based on manufacturer data, Energy Convers. Manage. 76 (2013) 137–144, http://dx.doi.org/10.1016/j.enconman.2013.07.042.

[95] Yukai Chen, E. Macii, M. Poncino, Frequency domain characterization of batteries for the design of energy storage subsystems, in: 2016 IFIP/IEEE International Conference on Very Large Scale Integration (VLSI-SoC). Presented At the 2016 IFIP/IEEE International Conference on Very Large Scale Integration, VLSI-SoC, IEEE, Tallinn, Estonia, 2016, pp. 1–6, http://dx.doi.org/10.1109/VLSI-SoC.2016.7753548.

[96] J. Wu, X. Zhang, Z. Ju, L. Wang, Z. Hui, K. Mayilvahanan, K.J. Takeuchi, A.C. Marschilok, A.C. West, E.S. Takeuchi, G. Yu, From fundamental understanding to engineering design of high-performance thick electrodes for scalable energy-storage systems, Adv. Mater. 33 (2021) 2101275, http://dx.doi.org/10.1002/adma.202101275.

[97] C. Lian, M. Janssen, H. Liu, R. van Roij, Blessing and curse: How a supercapacitor's large capacitance causes its slow charging, Phys. Rev. Lett. 124 (2020) 076001, http://dx.doi.org/10.1103/PhysRevLett.124.076001.

[98] J.A. Dowling, K.Z. Rinaldi, T.H. Ruggles, S.J. Davis, M. Yuan, F. Tong, N.S. Lewis, K. Caldeira, Role of long-duration energy storage in variable renewable electricity systems, Joule 4 (2020) 1907–1928, http://dx.doi.org/10.1016/j.joule.2020.07.007.

[99] M. Amiryar, K. Pullen, A review of flywheel energy storage system technologies and their applications, Appl. Sci. 7 (286) (2017) http://dx.doi.org/10.3390/app7030286.

[100] H.L. Ferreira, R. Garde, G. Fulli, W. Kling, J.P. Lopes, Characterisation of electrical energy storage technologies, Energy 53 (2013) 288–298, http://dx.doi.org/10.1016/j.energy.2013.02.037.

[101] G. Nagasubramanian, Electrical characteristics of 18650 Li-ion cells at low temperatures, J. Appl. Electrochem. 31 (2001) 99–104, http://dx.doi.org/10.1023/A:1004113825283.

[102] A. Chu, P. Braatz, Comparison of commercial supercapacitors and high-power lithium-ion batteries for power-assist applications in hybrid electric vehicles I. Initial characterization, J. Power Sources 112 (2002) 236–246, http://dx.doi.org/10.1016/S0378-7753(02)00364-6.

[103] S.S. Zhang, K. Xu, T.R. Jow, Charge and discharge characteristics of a commercial LiCoO2-based 18650 Li-ion battery, J. Power Sources 160 (2006) 1403–1409, http://dx.doi.org/10.1016/j.jpowsour.2006.03.037.

[104] P.L. Moss, G. Au, E.J. Plichta, J.P. Zheng, An electrical circuit for modeling the dynamic response of Li-ion polymer batteries, J. Electrochem. Soc. 155 (A986) (2008) http://dx.doi.org/10.1149/1.2999375.

[105] Y. Ji, Y. Zhang, C.-Y. Wang, Li-ion cell operation at low temperatures, J. Electrochem. Soc. 160 (2013) A636–A649, http://dx.doi.org/10.1149/2.047304jes.

[106] S.K. Kumar, A.A.B.M. Abduh, O. Sabih, R. Yazami, Temperature effect on Ragone plots of lithium-ion batteries, J. Electrochem. Soc. 165 (2018) A674–A679, http://dx.doi.org/10.1149/2.0591803jes.

[107] P. Braun, C. Uhlmann, M. Weiss, A. Weber, E. Ivers-Tiffée, Assessment of all-solid-state lithium-ion batteries, J. Power Sources 393 (2018) 119–127, http://dx.doi.org/10.1016/j.jpowsour.2018.04.111.

[108] M. Saakes, C. Kleijnen, D. Schmal, P. ten Have, Advanced bipolar lead–acid battery for hybrid electric vehicles, J. Power Sources 95 (2001) 68–78, http://dx.doi.org/10.1016/S0378-7753(00)00609-1.

[109] M. Ceraolo, G. Lutzemberger, D. Poli, C. Scarpelli, M. Sabatini, Experimental analysis of Ni-MH high power cells, in: 2020 55th International Universities Power Engineering Conference (UPEC). Presented At the 2020 55th International Universities Power Engineering Conference, UPEC, IEEE, Torino, Italy, 2020, pp. 1–6, http://dx.doi.org/10.1109/UPEC49904.2020.9209830.

[110] Y.V. Mikhaylik, J.R. Akridge, Low temperature performance of Li/S batteries, J. Electrochem. Soc. 150 (A306) (2003) http://dx.doi.org/10.1149/1.1545452.

[111] J.R. Akridge, Y.V. Mikhaylik, N. White, Li/S fundamental chemistry and application to high-performance rechargeable batteries, Solid State Ion. 175 (2004) 243–245, http://dx.doi.org/10.1016/j.ssi.2004.07.070.

[112] P.L. Moss, J.P. Zheng, G. Au, P.J. Cygan, E.J. Plichta, Transmission line model for describing power performance of electrochemical capacitors, J. Electrochem. Soc. 154 (A1020) (2007) http://dx.doi.org/10.1149/1.2778126.

[113] R. López-Vizcaíno, E. Mena, M. Millán, M.A. Rodrigo, J. Lobato, Performance of a vanadium redox flow battery for the storage of electricity produced in photovoltaic solar panels, Renew. Energy 114 (2017) 1123–1133, http://dx.doi.org/10.1016/j.renene.2017.07.118.

[114] L.F. Arenas, C. Ponce de León, F.C. Walsh, Redox flow batteries for energy storage: their promise, achievements and challenges, Curr. Opin. Electrochem. 16 (2019) 117–126, http://dx.doi.org/10.1016/j.coelec.2019.05.007.

[115] Q. Zhou, D. Du, C. Lu, Q. He, W. Liu, A review of thermal energy storage in compressed air energy storage system, Energy 188 (2019) 115993, http://dx.doi.org/10.1016/j.energy.2019.115993.

[116] T. Liang, A. Vecchi, K. Knobloch, A. Sciacovelli, K. Engelbrecht, Y. Li, Y. Ding, Key components for Carnot battery: Technology review, technical barriers and selection criteria, Renew. Sustain. Energy Rev. 163 (2022) 112478, http://dx.doi.org/10.1016/j.rser.2022.112478.

[117] M. Shanks, C.M. Shoalmire, M. Deckard, K.N. Gohil, H. Lewis, D. Lin, P.J. Shamberger, N. Jain, Design of spatial variability in thermal energy storage modules for enhanced power density, Appl. Energy 314 (2022) 118966, http://dx.doi.org/10.1016/j.apenergy.2022.118966.

[118] I. Beyers, A. Bensmann, R. Hanke-Rauschenbach, Energy-power relations and Ragone plots for packed bed thermal energy storage, in: Presented At the 36th International Conference on Efficiency, Cost, Optimization, Simulation and Environmental Impact of Energy Systems (ECOS 2023), ECOS 2023, Las Palmas De Gran Canaria, Spain, 2023, pp. 2138–2148, http://dx.doi.org/10.52202/069564-0193.

[119] W. Dreyer, J. Jamnik, C. Guhlke, R. Huth, J. Moškon, M. Gaberšček, The thermodynamic origin of hysteresis in insertion batteries, Nature Mater. 9 (2010) 448–453, http://dx.doi.org/10.1038/nmat2730.

[120] C. Pham, D. Månsson, Effects of smart meter privacy protection management on the lifetime performance of 18, 650 lithium-ion batteries, IET Smart Grid 5 (2022) 101–119, http://dx.doi.org/10.1049/stg2.12055.

[121] W.A. Appiah, J. Park, S. Song, S. Byun, M.-H. Ryou, Y.M. Lee, Design optimization of LiNi0.6Co0.2Mn0.2O2/graphite lithium-ion cells based on simulation and experimental data, J. Power Sources 319 (2016) 147–158, http://dx.doi.org/10.1016/j.jpowsour.2016.04.052.

[122] J.-S. Kim, D.-C. Lee, J.-J. Lee, C.-W. Kim, Optimization for maximum specific energy density of a lithium-ion battery using progressive quadratic response surface method and design of experiments, Sci. Rep. 10 (2020) 15586, http://dx.doi.org/10.1038/s41598-020-72442-4.

[123] F. Masseni, Optimal battery selection for hybrid rocket engine, in: Presented At the International Conference of Computational Methods in Sciences and Engineering, ICCMSE 2021, Heraklion, Greece, 2022, 050006, http://dx.doi.org/10.1063/5.0119295.

[124] T. Christen, C. Ohler, Optimizing energy storage devices using Ragone plots, J. Power Sources 110 (2002) 107–116, http://dx.doi.org/10.1016/S0378-7753(02)00228-8.